

1 **The Aare main overdeepening on the northern margin of the European Alps: Basins, riegels,**  
2 **and slot canyons**

3  
4 Fritz Schlunegger<sup>1</sup>, Edi Kissling<sup>2</sup>, Dimitri Bandou<sup>1,3</sup>, Guilhem Douillet<sup>1</sup>, David Mair<sup>1</sup>, Urs Marti<sup>4</sup>,  
5 Regina Reber<sup>1</sup>, Patrick Schläfli<sup>1,5</sup>, and Michael Schwenk<sup>1,6</sup>

6  
7 <sup>1</sup>Institute of Geological Sciences, University of Bern, Baltzerstrasse 1+3, 3012 Bern, Switzerland

8 <sup>2</sup>Department of Earth Sciences, ETH Zürich, Sonneggstrasse 5, 8092 Zürich, Switzerland

9 <sup>3</sup>Department of Environmental Sciences, University of Virginia, 291 McCormick Rd., Charlottesville,  
10 VA 22904-4123, USA

11 <sup>4</sup>Landesgeologie Swisstopo, Seftigenstrasse 264, Postfach, 3084 Wabern, Switzerland

12 <sup>5</sup>Institute of Plant Sciences and Oeschger Centre for Climate Change Research, Altenbergrain 21,  
13 3013 Bern, Switzerland

14 <sup>6</sup>Bayerisches Landesamt für Umwelt, Umweltdienstleistungen, Hof, 95030 Hof Saale, Germany

15  
16 [fritz.schlunegger@unibe.ch](mailto:fritz.schlunegger@unibe.ch)

Field Code Changed

17  
18 **Abstract**

19 This work summarizes the results of an interdisciplinary project where we aimed to explore the origin  
20 of overdeepenings through a combination of a gravimetry survey, drillings and dating. To this end, we  
21 focused on the Bern area, Switzerland, situated on the northern margin of the European Alps. This area  
22 experienced multiple advances of piedmont glaciers during the Quaternary glaciations, resulting in the  
23 carving of the main overdeepening of the Aare River valley (referred to as the Aare main  
24 overdeepening). This bedrock depression is tens of km long and up to several hundreds of m to a few  
25 km wide. We found that in the Bern area, the Aare main overdeepening is made up of two >200 m-deep  
26 troughs that are separated by a c. 5 km-long and up to 150 m-high transverse rocky ridge, interpreted  
27 as a riegel. The basins and the riegel are overlain by a >200 m- and a c. 100 m-thick succession of  
28 Quaternary sediments, respectively. The bedrock itself is made up of a Late Oligocene to Early Miocene  
29 suite of consolidated clastic deposits, which are part of the Molasse foreland basin. In contrast, the  
30 Quaternary suite comprises a middle Pleistocene to Holocene succession of unconsolidated glacio-  
31 lacustrine gravel, sand and mud. A synthesis of published gravimetry data revealed that the upstream  
32 stoss side of the bedrock riegel is c. 50% flatter than the downstream lee side. In addition, information  
33 from >100 deep drillings reaching depths >50 m suggests that the bedrock riegel is dissected by an  
34 anastomosing network of slot canyons. Apparently, the slot canyons established the hydrological  
35 connection between the upstream and downstream basins during their formation. Based on published  
36 modelling results, we interpret that the riegels and canyons were formed through incision of subglacial

37 meltwater during a glacier's decay state, when large volumes of meltwater were released. It appears  
38 that such a situation has repeatedly occurred since the Middle Pleistocene Transition approximately 800  
39 ka ago, when large, several hundreds of m-thick and erosive piedmont glaciers began to advance far  
40 into the foreland. This resulted in the deep carving of the inner-Alpine valleys and additionally in the  
41 formation of overdeepenings, riegels and slot canyons on the plateau situated on the northern margin of  
42 the Alps.

43

#### 44 **1 Introduction**

45 Overdeepenings are bedrock depressions below the current fluvial base-level (e.g., Jørgensen and  
46 Sandersen, 2006; Dürst Stucki et al., 2010; 2013; Fischer and Häberli, 2012). The downstream closures  
47 of these basins have adverse slopes that generally dip in the upstream direction (Häberli et al., 2016).  
48 Because bedrock depressions with such characteristics (Figure 1) are commonly found in previously  
49 glaciated areas, their formation has been interpreted as resulting from the erosional work of glaciers  
50 and/or subglacial meltwater (Wright, 1973; Herman and Braun, 2008; Egholm et al., 2009; Kehew et  
51 al., 2012; Patton et al., 2016; Liebl et al., 2023; and many others). Overdeepenings have been reported  
52 for the Quaternary from beneath the Greenland and Antarctic glaciers (Ross et al., 2011; Patton et al.,  
53 2016), but also in the North Sea (Moreau et al., 2012, Lohrberg et al., 2022), North America (Wright,  
54 1973; Lloyd et al., 2023) and northern Europe including Scandinavia (Clark and Walder, 1994;  
55 Piotrowski, 1997; Krohn et al., 2009). Glaciogenic paleovalleys are not only limited to the Quaternary  
56 but were also described for Paleozoic glaciations (e.g. Douillet et al., 2012; Dietrich et al., 2021). In the  
57 European Alps, such erosional troughs occur in Alpine valleys as well as on foreland plateaus on either  
58 side of this mountain belt (Preusser et al., 2010; Dürst Stucki and Schlunegger, 2013; Magrani et al.,  
59 2020). Pollen analysis (Welten, 1982; 1988; Schlüchter, 1989; Schläfli et al., 2021), dating using  
60 optically stimulating luminescence methods (Preusser et al., 2005; Dehnert et al., 2012; Büchi et al.,  
61 2018; Schwenk et al., 2022a) and <sup>14</sup>C ages established on organic matter encountered in the  
62 overdeepening fill (Kellerhals and Häfeli, 1984) showed that these troughs were formed after the Middle  
63 Pleistocene Transition, which occurred c. 800 ka ago (Schlüchter, 2004). Geophysical surveys (e.g.,  
64 Rosselli and Raymond, 2003; Reitner et al., 2010; Stewart and Lonergan, 2011; Stewart et al., 2013;  
65 Perrouy et al., 2015; Burschil et al., 2018; 2019; Ottesen et al., 2020) in combination with drillings  
66 (Jordan, 2010; Dürst Stucki et al., 2010; Büchi et al., 2017; 2018; Gegg et al., 2021; Bandou et al., 2022;  
67 2023; Anselmetti et al., 2022; Schwenk et al., 2022a, b; Gegg and Preusser, 2023; Schaller et al., 2023;  
68 [Schuster et al., 2024](#)) disclosed that such overdeepenings can be several km wide, tens of km long and  
69 >200 m deep. The surveys also showed that overdeepenings are typically composed of individual sub-  
70 basins, separated by bedrock swells or bumps oriented transverse to the flow of a former glacier,  
71 hereafter called riegels (Cook and Swift, 2012), yet the specific details of such a geometry have not yet  
72 been elaborated.

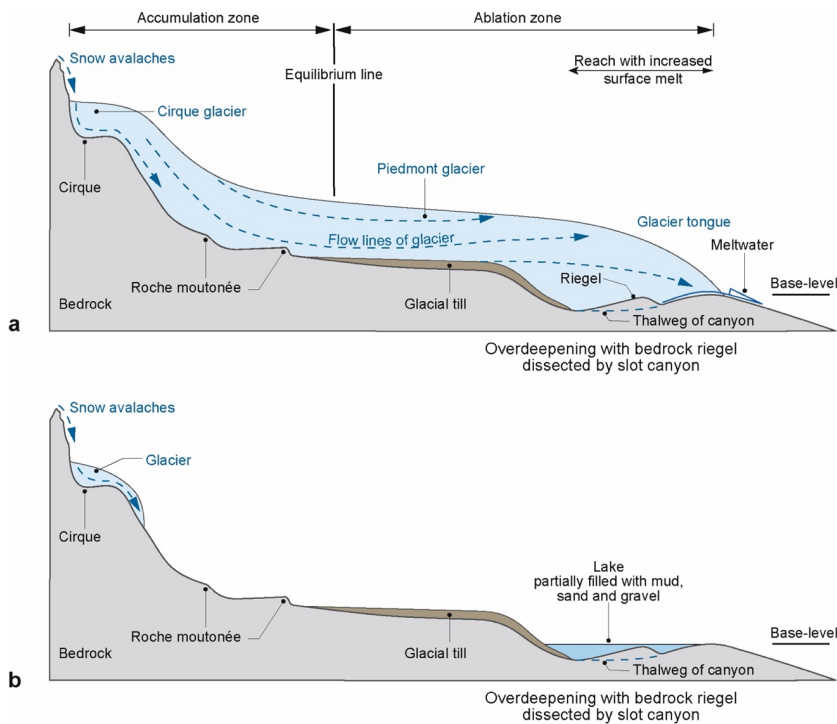


Figure 1

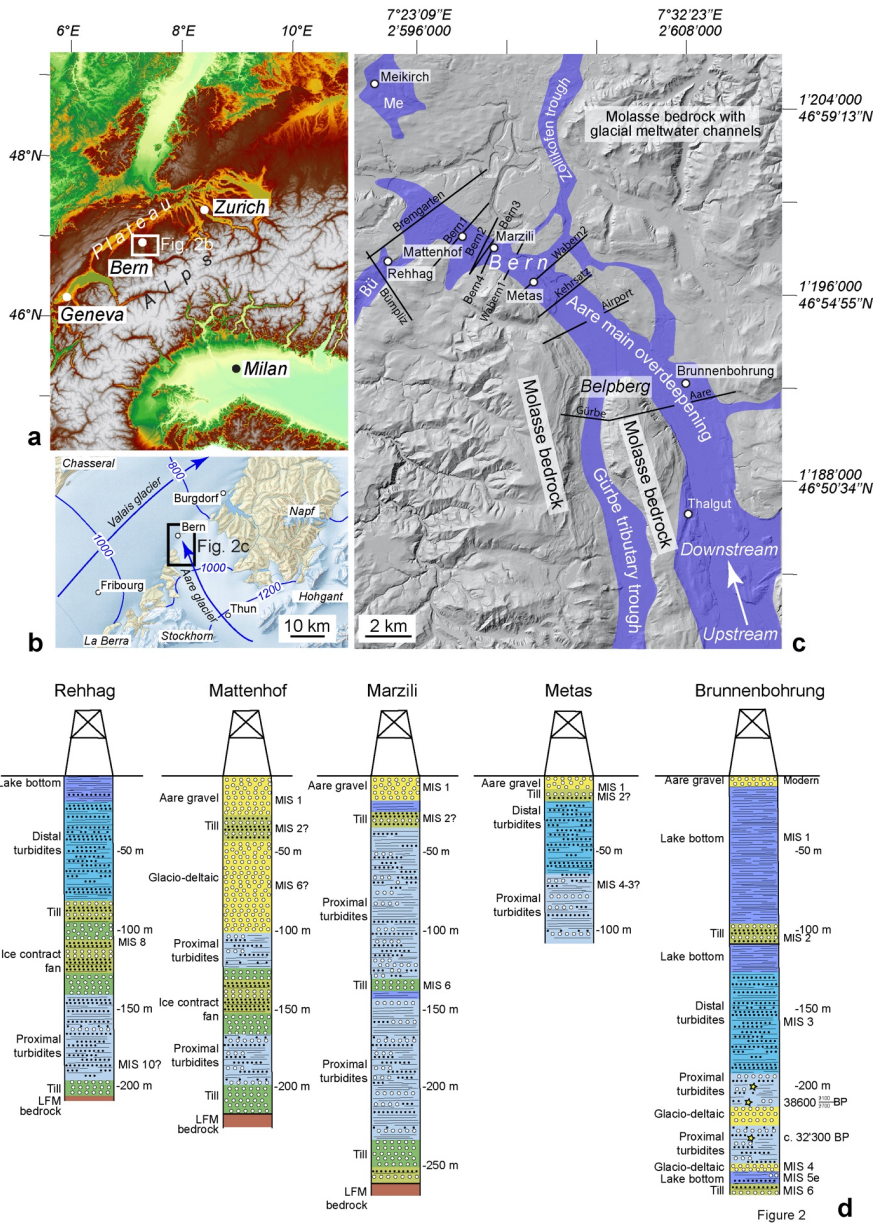
Figure 1: Architecture of a landscape sculpted by piedmont glaciers during glaciations. a) Situation immediately following a full glacial period during which a piedmont glacier, which extended far into the foreland, started to melt. As a result, large volumes of meltwater are produced in the ablation zone close to the glacier's tongue. This meltwater has the potential to contribute to the erosional downwearing of the bedrock, and it can cause the incision of canyons into bedrock riegels, which separate two overdeepened basins. b) During interglacial time periods, the piedmont glaciers disappear, and small ice caps may be preserved in the higher parts of a mountain belt. During this time, the overdeepened basin will be filled by lacustrine sediments and/or will eventually host a lake. Modified after Schlunegger and Garefalakis (2023).

73

74

75 Here, we summarize the results of an interdisciplinary project where we aim to explore the origin of  
 76 overdeepenings using a combination of data collected through a gravimetry survey (Bandou, 2023a;  
 77 Bandou et al., 2022, 2023), drillings (Reber and Schlunegger, 2016; Schwenk et al., 2022a, b) and  
 78 dating (Schläfli et al., 2021; Schwenk et al., 2022a). We focus our study on the Bern area situated on  
 79 the northern margin of the European Alps (Figure 2). For this region, we draw a map of the bedrock  
 80 topography combining the results of a gravimetry survey in the region (Bandou, 2023a; Bandou et al.,  
 81 2023) with information obtained through drillings. This map shows that an overdeepened trough or a  
 82 tunnel valley system, referred to as the Aare main overdeepening (Schwenk et al., 2022a), is made up  
 83 of two basins separated by a bedrock riegel, which itself is cut by one or multiple slot canyons. This

84 structure has a similar geometry as many examples reported from formerly glaciated landscapes  
 85 (Brocklehurst and Whipple, 2002; Brocklehurst et al., 2008) and particularly from Alpine valleys,  
 86 which points to similar processes resulting in their formation.



87

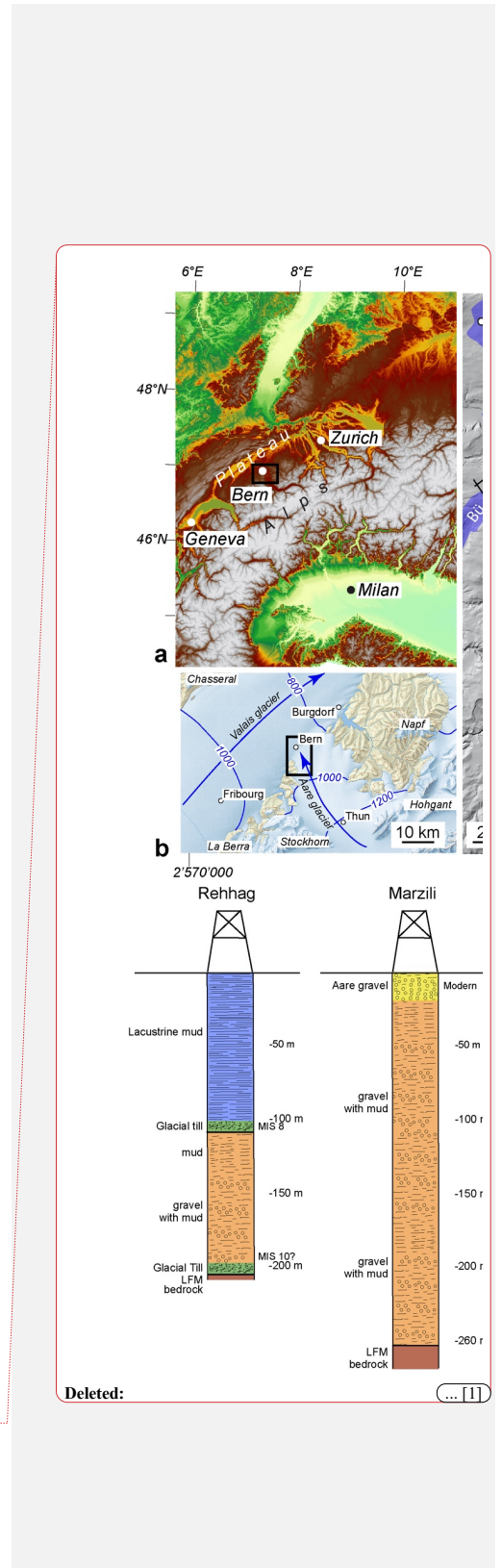


Figure 2: [Local setting illustrating the a\) Alpine arc \(modified from Bandou et al., 2023\) with latitudes and longitudes, b\) the study area during the Last Glacial Maximum \(LGM; map with isohypses of the glacier's surfaces taken from Bini et al., 2009\), c\) the surface geomorphology \(2 m-SwissAlti3D DEM © swisstopo\) together with the orientation of the Aare main overdeepening taken from Reber and Schlunegger \(2016\), and d\) information from drillings. The figure c\) shows \(i\) the sections along which gravity data was collected \(black lines: Bandou et al., 2022; 2023\), and \(ii\) the sites \(white circles\) where sediments in drillings \(Rehhag: Schwenk et al., 2022a, b; Meikirch: Welten, 1982; Preusser et al., 2005; Schläfli et al., 2021; Brunnenbohrung: Kellerhals and Häfeli, 1984; Zwahlen et al., 2021\) and exposures \(Thalgut: Welten, 1982; 1988; Schlüchter, 1989; Preusser and Schlüchter, 2004\) were either dated with various techniques, or where existing ages were reconfirmed by a subsequent analysis. Me=Meikirch overdeepening; Bü=Bümpliz trough. The numbers along the figure margin refer to the Swiss coordinate system \(CH1903+\) and are complemented with information on latitudes and longitudes. Panel d\) presents the logs of key drillings. The logs of the Brunnenbohrung \(modified after Kellerhals and Häfeli, 1984\) and Mattenhof drillings \(modified after Geotest, 2013\) were reconstructed from cuttings; the material at Metas and Rehhag was cored \(Geotest, 1997; Schwenk et al., 2022a\), whereas the sedimentary log of the Marzili drilling is based on a combination of cuttings and gamma ray data \(Gees, 1974\). The age models of the sequences encountered in the Mattenhof, Marzili, Metas and Brunnenbohrung drillings were based on regional correlations with dated horizons \(see Bandou et al., 2023, for further information\).](#)

91

92

## 93 **2 Setting**

### 94 *2.1 Overdeepened troughs in the Bern area*

95 The target overdeepening near Bern was sculpted by the Aare piedmont glacier with sources in the  
96 Central European Alps. From there, the Aare glacier flowed onto the Swiss Plateau (Figure 2a) over a  
97 distance of >20 km, and it merged with the Valais glacier north of Bern, at least during the Last Glacial  
98 Maximum (LGM) c. 20 ka ago (Figure 2b). Upstream of the city area of Bern, two bedrock depressions,  
99 referred to as the Gürbe tributary trough and the Aare main overdeepening (Figure 2c), form prominent  
100 basins. They are between c. 150 (Gürbe trough; Geotest, 1995) and >250 m deep (Aare main trough,  
101 Kellerhals and Häfeli, 1984), and several km wide (Bandou et al., 2022). Downstream of the city of  
102 Bern, the Aare main overdeepening splits into several tributary branches. Among these, the Bümpliz  
103 trough ('Bü' in Figure 2c) is the most prominent one with a depth >200 m (Schwenk et al., 2022a, b).  
104 The other depressions such as the Zollikofen trough are shallower and reach a depth of <150 m (Reber  
105 and Schlunegger, 2016). The study region also hosts the Meikirch overdeepening (labelled as 'Me' on  
106 Figure 3c), a nearly 200 m-deep trough (Dürst Stucki et al., 2010; Dürst Stucki and Schlunegger, 2003),  
107 which appears to be isolated from the rest of the overdeepening system (Reber and Schlunegger, 2016).  
108 Although the area between the northern termination of the Aare main overdeepening and the Meikirch  
109 trough is made up of exposed bedrock (Gerber, 1927), the possibility of a connection between both  
110 depressions via a narrow canyon, while quite unlikely according to Reber and Schlunegger (2016),  
111 cannot be completely ruled out. The Aare main overdeepening itself is the most prominent trough in  
112 the city area of Bern and has a maximum depth of nearly 250 m (Reber and Schlunegger, 2016).

113

114

115

116 2.2 *Chronologic framework of overdeepening fill*

117 The Quaternary fill of the Aare main overdeepening has been placed into the chronological framework  
118 of glacial advances onto the Swiss plateau during the past glaciations by previous authors. South of  
119 Bern, the Thalgut section (Figure 2c) disclosed the occurrence of pollen fragments embedded in a  
120 lacustrine sequence at the base and near the top of the section (Schlüchter, 1989). The pollen assemblage  
121 at the base was assigned to the Holsteinian interglacial period (Welten, 1982; 1988; Schlüchter, 1989;  
122 Preusser and Schlüchter, 2004), which either corresponds to MIS 9 (Roger et al., 1999) or MIS 11 (see  
123 discussion in Preusser et al., 2011; Koutsodendrīs et al., 2012; and Schwenk et al., 2022a for a  
124 discussion of ages). The lacustrine sediments near the top of the same suite were assigned to MIS 5e  
125 (Welten, 1982; 1988; Schlüchter, 1989). Approximately 6 km farther downstream of the Thalgut  
126 section, the Brunnenbohrung drilling (Figure 2d) penetrated nearly the entire sedimentary sequence of  
127 the Aare main overdeepening. Based on lithostratigraphic constraints and <sup>14</sup>C ages established on  
128 organic fragments, Kellerhals and Häfeli (1984) and subsequently Zwahlen et al. (2021) assigned an  
129 age postdating MIS 6 to the entire succession. Farther north of Bern, Schwenk et al. (2022a) used the  
130 results of feldspar luminescence dating to propose that the sedimentary suite penetrated by the Rehhag  
131 drilling has an age of MIS 8 and older (Figure 2d). *Finally, the Neubrügg section, which is exposed at*  
132 *the NE end of the Bremgarten profile (Figure 2a), exposes c. 60-70 m-thick sequence with a till at the*  
133 *base and the top. The succession also includes sand and gravel deposits with pollen fragments between*  
134 *the till layers, which may indicate the end of a warm period according to Lüthy et al. (1963). Bandou*  
135 *et al. (2023) used this information to suggest that the till at the base and the top of the suite could*  
136 *correspond to the MIS 6 and MIS 2 glaciations, respectively, while the sediments recording a warm*  
137 *period (or the end of a warm time interval) could have been deposited during MIS 5e. We acknowledge*  
138 *that all of the aforementioned* ages are not precise enough to reconstruct in detail the history of how and  
139 when the overdeepenings were formed, but they are consistent with the view that the deep troughs in  
140 the Bern area were originally formed after the Middle Pleistocene Transition c. 800 ka ago (Schlüchter,  
141 2004) and thus during the same period when the U-shaped Alpine valleys were carved (Häuselmann et  
142 al., 2007; Valla et al., 2011).

143  
144 2.3 *Lithological architecture of bedrock*

145 The bedrock in the region comprises an amalgamated suite of Early Miocene Upper Marine Molasse  
146 (UMM) sandstone beds south of Bern. Sedimentological analyses showed that these sediments were  
147 deposited in a shallow marine, mostly coastal environment (Garefalakis and Schlunegger, 2019). In the  
148 region north of Bern, the bedrock is made up of a Late Oligocene to Early Miocene suite of Lower  
149 Freshwater Molasse (LFM) sandstones and mudstones (Isenschmid, 2019). These sediments were  
150 deposited in a fluvial environment comprising channel fills and floodplains made up of sandstones and  
151 mudstones, respectively (Platt and Keller, 1992; Isenschmid, 2019). The bedding of the *Molasse*

Formatted: English (UK)

Formatted: English (UK)

Moved (insertion) [1]

Deleted: These

153 sediments and the contact between the UMM and the LFM gently dips towards the south by c. 10°  
154 (Isenschmid, 2019), with the consequence that south of Bern, the base of the Aare main overdeepening  
155 often consists of LFM deposits, while most of the upper part of the overdeepening is laterally bordered  
156 by bedrock made up of UMM. In addition, it has been postulated that the UMM sediments have a lower  
157 erodibility than the underlying LFM unit, based on the observation that the UMM forms a cap rock in  
158 the region (Isenschmid, 2019). Finally, Isenschmid (2019) documented that the Molasse bedrock  
159 beneath the Bern city area is dissected by left-lateral faults that strike NW-SE, offering zones of  
160 mechanical weaknesses.

161

#### 162 2.4 Lithological architecture of overdeepening fill

163 Schwenk et al. (2022a) grouped the Quaternary sediments recovered from the Rehhag drilling into  
164 distinct facies assemblages based on a detailed description of the 210 m-long drill core. The first  
165 assemblage, interpreted as subglacial traction till and encountered at the base of the Rehhag sequence  
166 (Figure 2d), comprises a suite of gravel with angular to rounded clasts that are embedded in a sandy to  
167 silty, strongly compacted and sheared matrix. This element shows strong lithologic similarities to the  
168 second facies assemblage, which consists of an alternation of gravel and sand layers and which was  
169 encountered in the middle of the drill core. This assemblage was interpreted by Schwenk et al. (2022a)  
170 as ice contact fan deposits. Finer-grained facies assemblages consist either of (i) sand layers with mud  
171 and gravel interbeds (in the section between c. 195 and 140 m depth), interpreted as deposits from  
172 proximal turbidity currents, or of (ii) alternating sand and mud layers (in the section between c. 80 and  
173 20 m depth), representing deposits from distal turbidity currents (Figure 2d). The uppermost sequences  
174 made up of mud layers with isolated clasts (drop stones) were interpreted as lake bottom sediments  
175 (Figure 2d). Based on OSL dating, Schwenk et al. (2022a) assigned a MIS 8 or possibly older age to  
176 the sequence at the Rehhag.

177 At the Mattenhof situated farther to the ENE, the log of the >200 m-thick Quaternary sequence was  
178 reconstructed based on cuttings (Geotest, 2013). The suite starts with a c. 20 m-thick gravel, which is  
179 overlain by a c. 30 m-thick succession of mud with gravel interbeds. Following the scheme of Schwenk  
180 et al. (2022a), we interpret this sequence as a till that is overlain by material supplied by turbidites  
181 (Figure 2d). The following sequence between 166 and 124 m drilling depth comprises gravel beds with  
182 mud and interbedded sand layers. This represents a more proximal facies than the underlying sequence  
183 and could, according to the interpretation scheme of Schwenk et al. (2022a), correspond to ice-contact  
184 fan deposits. The overlying suite, up to a depth of 102 m, is made up of mud with some gravel layers  
185 and isolated clasts. Similarly to the basal unit, this material was most likely supplied by turbidity  
186 currents. The isolated clasts in this suite could represent drop stones. The upper part of the Mattenhof  
187 section consists of gravel deposits up to a depth of 42 m, followed by a silty gravel unit between 42 and  
188 28 m depth, and then another gravel sequence reaching the top of the section. This gravelly suite could

**Deleted:** Detailed information on the lithologic architecture of the overdeepening fill is available from a few drillings only (Figure 2d). South of Bern, the >250 m-thick succession at the Brunnenbohrung site starts with a few meters of till (possibly MIS 6), yet the drilling did not reach the bedrock. The till is overlain by a several m-thick lacustrine silt (possibly MIS 5e) and a >100 m-thick sequence made up of fluviolacustrine gravel, dated to MIS 3 based on <sup>14</sup>C concentrations in organic matter (Kellerhals and Häfeli, 1984). The topmost 100 m-thick suite comprises a till at its base (possibly MIS 2) and a monotonous succession of lacustrine mud topped by a fluvial gravel.

201 potentially represent a glacio-deltaic system, postdating MIS 6 according to the regional correlation of  
 202 Bandou et al. (2023).

203 For the Marzili drilling, information about the stratigraphic architecture of the >250 m-thick Quaternary  
 204 suite was reconstructed based on cutting and gamma ray data (Gees, 1974). There, the sequence starts  
 205 with suite made up of gravels and interbedded sand layers, which we interpret as a till or as ice contact  
 206 fan deposits following the interpretation scheme of Schwenk et al. (2022a). These deposits are overlain  
 207 by a sequence of mud with interbedded gravel layers, possibly representing an environment where a  
 208 large portion of the material was supplied by turbidity currents. A 4 m-thick gravel unit was encountered  
 209 at a drilling depth of c. 130, which could represent a till. The overlying sequence comprises an  
 210 alternation of gravel and mud (Gees, 1974), possibly representing a suite of sediments supplied by  
 211 turbidity currents. Towards the top, the Marzili section comprises a 6 m-thick sequence made up of  
 212 mud, and it ends with a 20 m-thick fluvial gravel. Based on regional correlations, Bandou et al. (2023)  
 213 tentatively assigned a post-MIS 6 age to the sequence overlying the gravel at the depth of 130 m.

214 Farther north, the Metas drilling penetrated a 110 m-thick sequence without reaching the bedrock  
 215 (Geotest, 1997). The drilled core starts with a c. 90 m-thick suite made up of mud and sand layers,  
 216 which contains isolated clasts. These sediments were most likely deposited in a proglacial lake, by  
 217 turbidity currents. In this context, the isolated clasts could represent drop stones (Schwenk et al., 2022a).  
 218 This sequence is overlain by a till (MIS 2?) and finally by a c. 15 m-thick proglacial gravel (Geotest,  
 219 1997). Finally, south of Bern, the >250 m-thick succession at the Brunnenbohrung site (log based on  
 220 cuttings) starts with a few m-thick till (possibly MIS 6), yet the drilling did not reach the bedrock  
 221 (Kellerhals and Häfeli, 1984). The till is overlain by a several m-thick alternation of mud, silt and sand  
 222 layers (possibly MIS 5e). The latter unit is then followed by a >30 m-thick suite made up of a glacio-  
 223 deltaic gravel, alternations of gravel, mud and sand, and then again by a 10 m-thick gravel. It continues  
 224 with a fining-upward sequence deposited by turbidity currents at the bottom of a lake. Measurements  
 225 of <sup>14</sup>C concentrations in organic matter point to an age of MIS 3 (Kellerhals and Häfeli, 1984). The  
 226 topmost 100 m-thick suite starts with a till at a depth of c. 100 m (possibly MIS 2), which grades into a  
 227 fining-up sequence made up of mud and silt deposited at the bottom of a lake. The Brunnenbohrung  
 228 section ends with a fluvial gravel.

229 In summary, the Quaternary successions are spatially highly heterogeneous as disclosed by the drillings,  
 230 but they all record the same depositional setting as the sediments were most likely deposited in a glacio-  
 231 lacustrine environment (e.g., Schwenk et al., 2022a). Apparently, the material supply was spatially  
 232 highly heterogeneous (Schwenk et al., 2022b) as evidenced by the varying locations where coarse-  
 233 grained facies assemblages were encountered in the drillings (Figure 2d).

- Deleted: It
- Deleted: contain
- Deleted: . It
- Deleted: A similar sedimentologic architecture, based on cutting and gamma ray data, was also inferred for the Quaternary suite penetrated by the Marzili drilling situated in the city area of Bern (Gees, 1974).
- Deleted: the Rehthag drilling, which was sunk into the Bümpliz tributary trough and which reached the bedrock (Schwenk et al., 2022a), unraveled a 210
- Deleted: of Quaternary sediments. The Quaternary suite
- Formatted: Font: Times
- Formatted: Font: Times, English (UK)
- Deleted: , which
- Formatted: Font: Times, English (UK)
- Deleted: c. 100
- Deleted: sequence
- Formatted: Font: Times, English (UK)
- Formatted: Font: Times, English (UK)
- Formatted: Font: Times, English (UK)
- Deleted: gravel
- Formatted: Font: Times, English (UK)
- Deleted: . A second till was identified at a drilling depth of 103 m. It
- Deleted: overlain
- Formatted: Font: Times, English (UK)
- Deleted: succession of mud
- Formatted: Font: Times, English (UK)
- Deleted: isolated pebbles,
- Deleted: in a proglacial
- Deleted: Apparently
- Formatted: Font: Times, English (UK)
- Formatted: Font: Times, English (UK)
- Formatted: Font: Times, English (UK)
- Formatted: English (UK)
- Deleted: Schwenk et al., 2022a).
- Formatted: English (UK)



260 2.5 *Density of Molasse bedrock and Quaternary sediments*

261 Data on the bulk density of the Molasse bedrock and the overlying Quaternary sediments is crucial for  
262 interpreting gravimetric datasets (Kissling and Schwendener, 1990). In this context, Schwenk et al.  
263 (2022a), Schaller et al. (2023) and Schuster et al. (2024) measured  $\gamma$ -density values on drill cores with  
264 a multi-sensor core logger. Their results revealed a strong dependence of the material densities on  
265 lithology, with the largest density values measured for gravel layers. Yet in addition to lithological  
266 control, Schwenk et al. (2022a) showed that the measured density values generally increase with the  
267 depth at which the Quaternary sequences were deposited, indicating that post-depositional compaction  
268 also played a role in determining the density of the Quaternary sediments (Schwenk et al., 2022a).  
269 However, for interpreting the gravity signal of Quaternary sediments, the bulk density of the entire  
270 sedimentary suite is more diagnostic than the density values of individual sedimentary beds (Kissling  
271 and Schwendener, 1990). Such bulk density values were determined by Bandou et al. (2022) for the  
272 Molasse bedrock and the Quaternary sediments overlying the overdeepened troughs using the results of  
273 a Nettleton profile across the Belpberg mountain (that is underlain by Molasse bedrock, Figure 2c), and  
274 through 3D gravity modelling. Using this approach, these authors assigned a bulk density of 2500 kg/m<sup>3</sup>  
275 to the Molasse units (Figure 2c). This is a substantially higher value than the bulk densities between  
276 2150 and 2000 kg/m<sup>3</sup>, which have been determined for the basal part and the top sequences of the  
277 Quaternary suites in the Aare main overdeepening, respectively. In particular, Bandou et al. (2023)  
278 documented that the best-fit reproduction of the gravity signals along the Bremgarten, Bern1, Bern2  
279 and Kehrsatz profiles could be achieved by assigning a density value of 2000 kg/m<sup>3</sup> to the topmost  
280 sediments postdating MIS 6, and a higher density of approximately 2150 kg/m<sup>3</sup> (due to a greater  
281 compaction) to the underlying Quaternary deposits predating MIS 6. Drilling information (Mattenhof,  
282 Marzili, Metas) shows that the sediments younger than MIS 6 comprise a suite made up of gravels  
283 (Mattenhof), alternations of gravel, mud and sand beds (Marzili) and mud with interbedded sand layers  
284 (Metas). The results thus indicate that the bulk densities of the Quaternary sediments depend less on the  
285 lithological architecture of the material or the depositional environment in which the sediments were  
286 deposited. Instead, they appear to be primarily influenced by the overburden of the overdeepening fill  
287 and the number of glaciations, during which the Quaternary sediments were compacted under a thick  
288 glacial cover (Bandou et al., 2023). For instance, a sequence postdating MIS 6 was compacted by a  
289 pedmont glacier during the Last Glacial Maximum (LGM) only, while the older sediments experienced  
290 a glacial compaction during at least two full glaciations.

291 ▼  
292 2.6 *Riegels and slot canyons in Alpine valleys*

293 Bedrock swells between neighbouring basins are common features in previously glaciated landscapes  
294 (Anderson et al., 2006; Alley, 2019). They are common in the European Alps (see Figure 3, for a few  
295 examples), and they have also been detected underneath active glaciers (Feiger et al., 2018; Nishiyama

Formatted: English (UK)

Deleted: For the Bern region,

Moved up [1]: Bandou et al.

Deleted: (2022) used

Deleted: ) to assigne

Deleted: These density values were measured with a multi sensor core logger on the core of the Rehhag drilling (Schwenk et al., 2022a) and obtained through 3D gravity modelling along several profiles in the Bern area (Bandou et al., 2022; 2023a). The results showed

Deleted: are

Deleted: a function of

Deleted: maximum depth

Deleted: (2023).

Deleted: ¶

¶

311 et al., 2019). In the Alps, most of the bedrock swells cross the thalweg of valleys (Figure 3) and are  
 312 dissected by inner gorges or slot canyons that connect the upstream with the downstream basin (Hantke  
 313 and Scheidegger, 1973; Valla et al., 2010; Montgomery and Korup, 2011). In addition, Alpine bedrock  
 314 riegels have a geometry where the upstream stoss side is flatter than the downstream lee side (insets of  
 315 Figure 3). This is particularly the case for the swells in (Figure 3): the Aare valley (Figure 3a; dip of  
 316 stoss side and lee sides  $<5^\circ$  and  $>6^\circ$ , respectively; Hantke and Scheidegger, 1973), the Trift valley  
 317 (Figure 3b; c.  $30^\circ$  versus  $40^\circ$ ; Steinemann et al., 2021), and the Maggia valley (Figure 3c;  $6^\circ$  versus  
 318  $40^\circ$ ). Bedrock riegels and slot canyons are also found on the foreland plateau adjacent to the Alps such  
 319 as the example east of Lucerne (Figure 3d), yet their geometric expressions are less well-developed. In  
 320 this work, we will document that the overdeepening beneath the city of Bern shares the same geometric  
 321 properties as the ensemble of bedrock riegels and slot canyons in Alpine valleys.

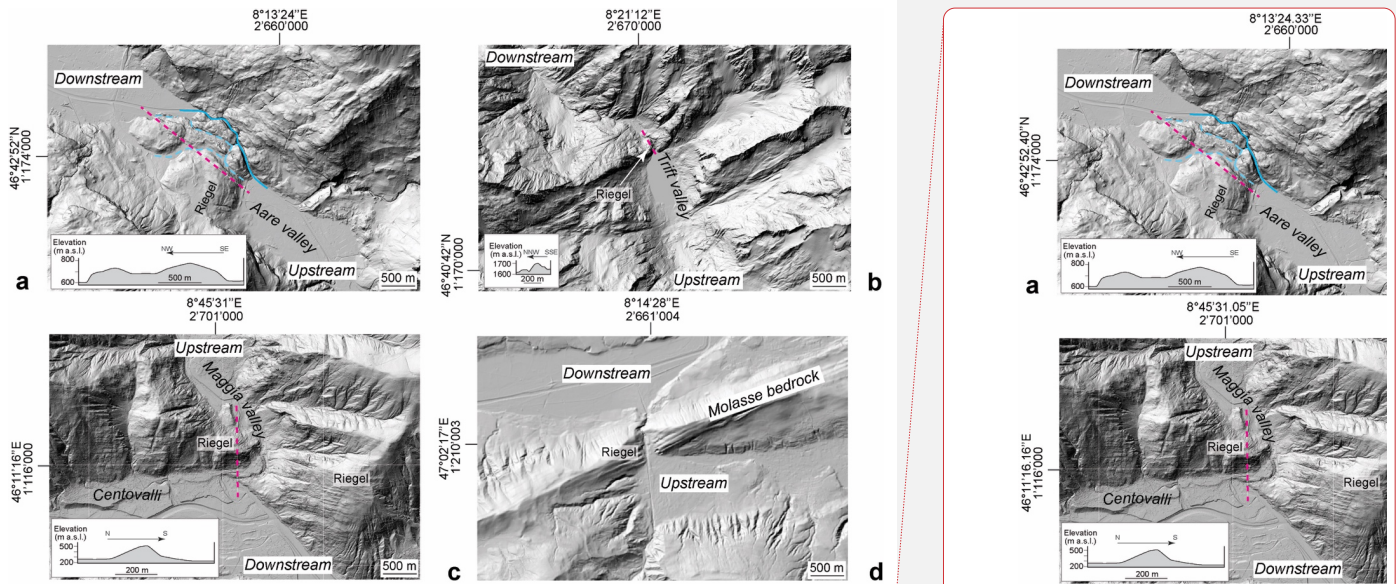


Figure 3

Figure 3: Hillshade 2 m-SwissAlti3D DEM (© swisstopo) illustrating examples in Alpine valleys where bedrock riegels separate overdeepened basins situated farther upstream and downstream. The insets illustrate topographic sections across the riegels, and the arrows display the flow direction of the glaciers during a glaciation. The coordinates refer to the Swiss coordinate system (CH1903+). Longitudes and latitudes are also indicated.

323

### 324 3 Dataset and Methods

325 The bedrock topography beneath the city area of Bern was already reconstructed in 2010 and then  
 326 updated in 2016, based on information from thousands of drillings publicly available on the Geoportal  
 327 of the Canton Bern (see Dürst Stucki et al. (2010), and Reber and Schlunegger (2016), respectively).

Deleted:

329 Since these drillings primarily penetrated the entire Quaternary sequence down to the bedrock at the  
330 lateral margins of the Aare main overdeepening, we consider the bedrock topography model of Reber  
331 and Schlunegger (2016) for the shallow parts of the trough as accurate. Yet detailed reconstructions of  
332 the deeper, central part of the overdeepening were hindered due to a lack of information from deep  
333 drillings at that time (Reber and Schlunegger, 2016). Here, we benefit from the results of a recent gravity  
334 survey conducted in the city area of Bern (Bandou et al., 2022; 2023; Bandou, 2023a) and information  
335 from new drillings >50 m deep. We proceeded through compiling, as a first step, the publicly available  
336 gravity data. We re-processed them to provide information about the spatial pattern of the gravity signal,  
337 either from the bedrock topography beneath the overdeepening fill (section 3.1) or from the  
338 overdeepening fill itself (section 3.2). Using these data along with the results from modelling conducted  
339 by Bandou et al. (2023), we reconstructed a map outlining the general thickness distribution of the  
340 Quaternary sediments (section 3.3). This was then used as the basis to update the existing bedrock  
341 topography model of Reber and Schlunegger (2016), thereby incorporating data from >100 drillings  
342 that penetrated >50 m into the subsurface (section 3.4).

343

### 344 3.1 *Assessing the gravity signal of the bedrock topography beneath the overdeepening*

345 We compiled the gravity data collected by Bandou (2023a) and combined them with data archived in  
346 the Gravimetric Atlas of Switzerland by Swisstopo (Olivier et al., 2008; 2011). From this dataset, we  
347 calculated the Bouguer anomaly values (see Bandou et al., 2023, for references to the methodological  
348 papers) using the density of the Molasse bedrock (2500 kg/m<sup>3</sup>) instead of the standard density of 2670  
349 kg/m<sup>3</sup> that is conventionally used for Bouguer anomaly corrections. We then draw the isogals (contour  
350 lines of equal Bouguer anomaly values) using the Golden Software Surface licensed to Swisstopo. This  
351 map was used to infer the general shape of the bedrock topography beneath the overdeepening fill. In  
352 particular, deviations of the isogals from the long-wavelength trend can serve as *a-priori* constraints for  
353 reconstructing the course and geometry of the bedrock outlining the overdeepening.

354

### 355 3.2 *Assessing the gravity signal of the Quaternary sediments overlying the overdeepening*

356 Subtracting the Bouguer anomalies values measured along a profile from the regional gravity field along  
357 the same profile yields what is referred to as the residual gravity anomaly. The related values provide  
358 information about a near-surface body or structure with a bulk density different from that of the  
359 surrounding bedrock (Kissling and Schwendener, 1990). Bandou et al. (2022; 2023) used this concept  
360 to determine the gravity signal of the Quaternary sediments overlying the Molasse bedrock. They  
361 proceeded by calculating the residual gravity anomaly values along 10 profiles perpendicular to the  
362 inferred course of the Aare main overdeepening (black lines in Figure 2c). Note that because the  
363 Quaternary deposits have a lower bulk density than the Molasse bedrock, the occurrence of such  
364 deposits results in a negative residual gravity anomaly (Kissling and Schwendener, 1990). Accordingly,

Formatted: English (UK)

Formatted: English (UK)

Formatted: English (UK)

Formatted: English (UK)

Field Code Changed

365 a larger bulk mass of Quaternary sediments yields a stronger (and thus a more negative residual  
366 anomaly) signal than a fill with less Quaternary material (Kissling and Schwendener, 1990; Bandou et  
367 al., 2022). Following this concept, we compiled the residual anomaly data from Bandou et al. (2023)  
368 for each gravity profile and drafted a contour map where each line displays the same residual anomaly  
369 value. This map was drawn by hand, thereby considering the *a-priori* information about the orientation  
370 of the Aare main overdeepening (Reber and Schlunegger, 2016).

371

### 372 3.3 *Estimating the thickness of Quaternary sediments based on gravity data*

373 Residual gravity anomaly values can be converted to thicknesses of Quaternary sediments through  
374 modelling, provided that *a-priori* data is available (Kissling and Schwendener, 1990). This includes  
375 information on: (i) density contrasts between the Molasse bedrock and the Quaternary fill, (ii) depths  
376 of bedrock encountered in drillings, and (iii) an already existing bedrock topography model (in our case  
377 the bedrock topography model of Reber and Schlunegger, 2016). Bandou et al. (2023) used a 3D gravity  
378 software referred to as PRISMA (Bandou, 2023b) to implement this approach, modelling the residual  
379 gravity anomalies along six profiles (Figure 5b) where the aforementioned *a-priori* data is well  
380 constrained. Note that upon using PRISMA, the geometry of the overdeepening fill was approximated  
381 by Bandou et al. (1922, 1923) through multiple right-handed prisms oriented as perpendicularly as  
382 possible to the profile of interest (Nagy, 1966; Banerjee and Das Gupta, 1977). We compiled the results  
383 of the PRISMA modelling presented by Bandou et al. (2022, 2023) to draw a map displaying the  
384 thickness distribution of Quaternary sediments overlying the Aare main overdeepening. When creating  
385 this map, we considered that a trend towards smaller or larger negative residual anomalies indicates a  
386 thinning or thickening of the Quaternary sediments, respectively (Kissling and Schwendener, 1990;  
387 Bandou et al., 2023). The difference between the elevation of the modern topography and the thickness  
388 of the Quaternary sediments returns a map displaying the bedrock topography.

389

### 390 3.4 *Combining the results of the gravity survey with drilling data to reconstruct the details of the* 391 *bedrock topography*

392 We updated the bedrock model of Reber and Schlunegger (2016) with information about the general  
393 shape of the overdeepening retrieved through gravity modelling outlined above, and we additionally  
394 considered the information of >100 drillings that were sunk >50 m deeply into the subsurface during  
395 the past years. Similar to Reber and Schlunegger (2016), we manually drew the isohypses of the  
396 bedrock, inferring that changes in the orientation of the contour lines and the depths of the bedrock were  
397 gradual. We finally combined the map displaying the geometry of the bedrock beneath the  
398 overdeepening with the elevation data provided by the 2 m-SwissAlti3D DEM (based on LIDAR data  
399 of [Swisstopo](#)) to present the shape of the bedrock topography as shaded relief.

Formatted: English (UK)

Deleted: swisstopo

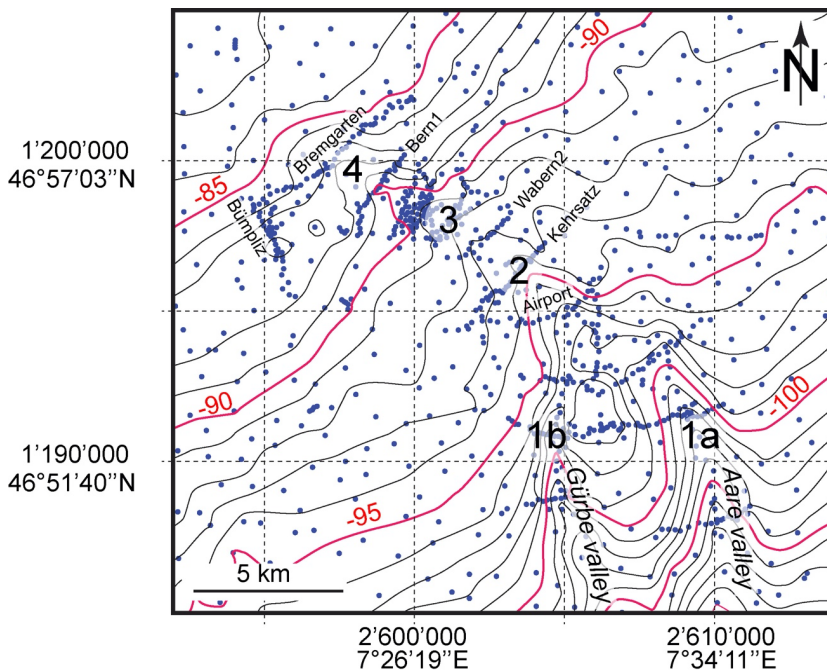
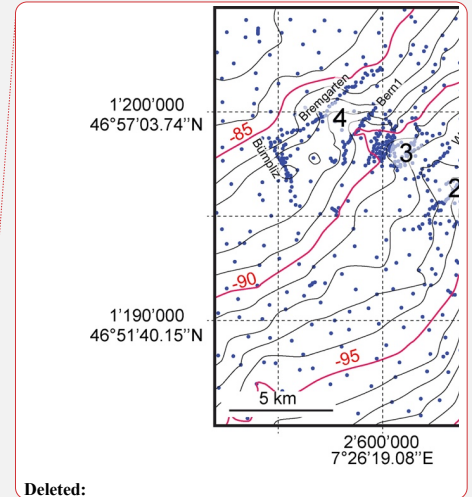


Figure 4

Figure 4: Bouguer anomalies, calculated with the density of the Molasse bedrock ( $2500 \text{ kg/m}^3$ ). The blue dots are gravity data taken from the Gravimetric Atlas of Switzerland (Olivier et al., 2008; 2011; [Swisstopo](#)) and from Bandou (2023a). The isogals, indicated in mGal, illustrate the general gravity trend in the region and deviations thereof. 1a and 1b are sites located in the Aare and Gürbe valleys, respectively. These are the locations where the isogals have the largest deflections from the large-wavelength trend. Farther to the N (site 2) and then to the NW, the deflections decrease, reaching the lowest values at site 3. They increase again towards site 4 and then fade towards the NW. The figure also shows the locations of the gravity profiles presented in Bandou (2022) and Bandou et al. (2023). The grid corresponds to the Swiss coordinate system (CH1903+). Longitudes and latitudes are also indicated.



Deleted:

Field Code Changed

Deleted: swisstopo

402

## 403 4 Results

### 404 4.1 Isogals and gravity signal of the bedrock topography beneath the overdeepening

405 The isogals calculated with the density of bedrock ( $2500 \text{ kg/m}^3$ ) clearly depict the general gravity trend,  
 406 which is characterized by a continuous SE-directed increase of the Bouguer anomaly values from -85  
 407 mGal in the NW to -105 mGal towards the SE (Figure 4). Note that a more negative value implies a  
 408 stronger gravity anomaly. The isogals generally strike SW-NE, reflecting the orientation of European  
 409 continental lithosphere, which gently dips beneath the Alpine orogen. However, and most importantly  
 410 in our context, the isogals also deviate from this pattern by being deflected towards the NW, where we  
 411 expect the occurrence of the Gürbe tributary trough and the Aare main overdeepening. This anomaly  
 412 (or deflection) has indeed the largest amplitudes of  $>4 \text{ mGal}$  and  $>3 \text{ mGal}$  beneath the Aare (location

414 1a on Figure 4) and Gürbe valleys, respectively (location 1b). This indicates that the depth of the  
 415 overdeepened trough is greatest there. Farther to the NW, the amplitude of the deflection decreases from  
 416 approximately 3 mGal at site 2 (between Airport and Kehrsatz) to <1 mGal at site 3 (Figure 4),  
 417 suggesting a shallowing of the bedrock trough and thus the occurrence of a swell (or riegel). From there,  
 418 the amplitude increases again at site 4 as the trough appears to deepen once more, after which the  
 419 anomaly fades farther to the NW.

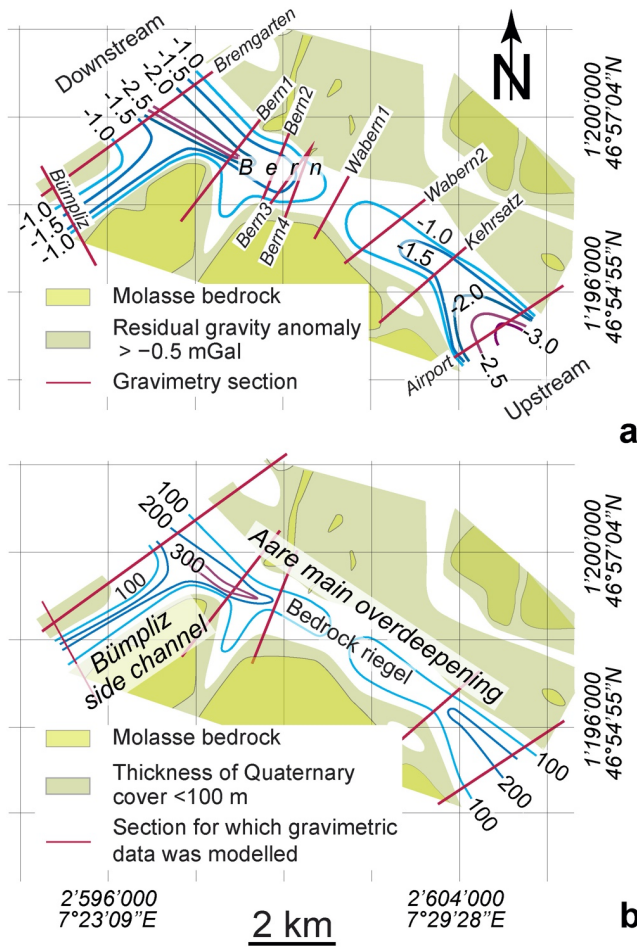
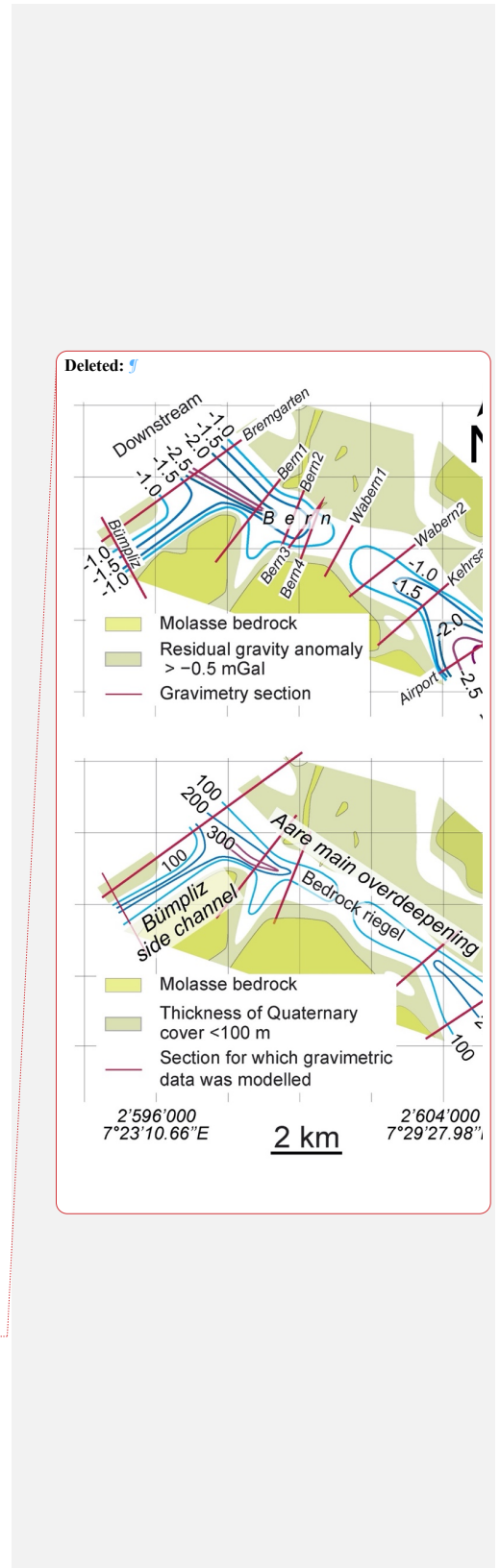


Figure 5



420

Figure 5: Residual gravity anomalies, representing the gravity signal of Quaternary sediments, and inferred thicknesses of Quaternary deposits. a) The contour lines of the residual gravity signals (mGal) caused by the Quaternary fill of the Aare main overdeepening are mainly based on gravity surveys along 10 sections (red lines; Bandou et al., 2023). Here, more negative values imply a greater signal caused by the bulk mass of Quaternary sediments overlying the overdeepened trough (Kissling and Schwendener, 1990; Bandou et al., 2022). b) Spatial distribution of Quaternary sediments, here expressed by the related thicknesses. These are mainly based on the results of gravity modelling, where Quaternary mass and its spatial distribution was forward modelled until a best-fit between the modelled and observed gravity signals of the Quaternary mass overlying the overdeepened trough was reached (Bandou, 2023; Bandou et al., 2023). Note that only the residual gravity anomalies of the Airport, Kehrsatz, Bern2, Bern1, Bremgarten and Bümpliz sections were modelled by Bandou et al. (2023). The grid refers to the Swiss coordinate system (CH1903+). Longitudes and latitudes are also indicated.

423

#### 424 4.2 Gravity signals of the Quaternary sediments overlying the overdeepening

425 The residual gravity anomalies, which correspond to the gravity signal of the Quaternary sediments,  
426 reveal the same pattern as the isogals where the Bouguer anomaly values were calculated with the  
427 bedrock density of 2500 kg/m<sup>3</sup>. For the section across the Gürbe and Aare valleys (Figure 2c), Bandou  
428 et al. (2022; 2023) showed that the Quaternary fill of the Aare main overdeepening results in a gravity  
429 signal that ranges between c. -4.0 and -0.5 mGal. In addition, they showed that this signal changes from  
430 upstream to downstream: In particular, along the Gürbe-Aare transect (Figure 2c), which also crosses  
431 the Belpberg mountain ridge made up of Molasse bedrock, the strength of the signal ranges from c. -  
432 2.9 mGal in the Gürbe valley to c. -4.1 mGal in the Aare valley (Bandou et al., 2022). Farther  
433 downstream, the residual anomaly values and thus the signal of the overdeepening fill decreases, where  
434 the corresponding values change from c. -3.0 mGal (Airport profile) to approximately -1.5 and finally  
435 c. -1.0 mGal along the Kehrsatz and Wabern2 profiles, respectively (Figure 5a). The weakest signals  
436 with values between c. -0.5 mGal and -1 mGal were reported for the Wabern1 profile (Bandou et al.,  
437 2023; Figure 5a). This suggests a decrease in the mass of Quaternary sediments approaching Wabern1,  
438 most likely due a shallowing of the bedrock forming a riegel in this area. Farther downstream, the  
439 gravity signal of the Quaternary fill increases again and reaches values between c. -1.0 and c. -2.0 mGal  
440 along the Bern sections, and then approximately -2.5 mGal along the Bremgarten section c. 2 km farther  
441 downstream. This points towards an increase in the Quaternary mass and thus towards a deepening of  
442 the trough in this direction. The residual anomaly data thus clearly depict the course of the Aare main  
443 overdeepening, which strikes SE-NW in the city area of Bern (Figures 2c, 5a). Towards the NW margin  
444 of the study area, a second overdeepening referred to as the Bümpliz tributary trough (Schwenk et al.,  
445 2022a) strikes SW-NE and converges with the Aare main overdeepening NW of Bern. The gravity  
446 signal of the Bümpliz sedimentary fill is less and reaches a value of c. -1.5 mGal (Figure 5a; Bandou et  
447 al., 2023). Finally, the upstream side of the inferred bedrock riegel dips gentler than the downstream  
448 side, which is twice as steep: on the stoss side, the residual gravity anomalies change from <-2.5 mGal  
449 to >-1.0 mGal over a downstream distance of c. 4 km whereas on the lee side, the same change in the  
450 gravity signal occurs over only 2 km. Given that the residual gravity signal is a direct response of the  
451 bulk mass of Quaternary sediments overlying the Molasse bedrock (see section 4.2), and thus their

452 volume supposing a lower density than the Molasse bedrock (see next section and Bandou et al., 2022;  
453 2023), the differences in the upstream and downstream gradients of the residual gravity anomaly values  
454 disclose the contrasts in the dip angles of the bedrock topography.

455

#### 456 4.2 *Thickness of Quaternary sediments*

457 Available drilling information shows that the Quaternary fill in the Bern region generally consists of an  
458 alternation of gravel, sand and mud (Figure 2d), which have a bulk density that ranges from 2150 kg/m<sup>3</sup>  
459 for material at the base of the overdeepening fill, to 2000 kg/m<sup>3</sup> for the sediments towards the top,  
460 [\(Bandou et al., 2023\)](#). Based on a sensitivity analysis where the gravity response to different densities  
461 for the Quaternary sediments was evaluated, Bandou (2023a) and Bandou et al. (2022, 2023) could  
462 exclude the possibility that the Bouguer anomaly and residual anomaly patterns displayed in Figures 4  
463 and 5a could be explained by spatial differences in the sedimentary architecture of the Quaternary fill.  
464 For instance, the low residual gravity anomalies displayed in the region of the Wabern2 profile (Figure  
465 5a) would require an amalgamation of highly compacted glacial till. However, this is not consistent  
466 with the stratigraphic log of the core drilled at Metas (Figure 2d), which is made up of an alternation of  
467 sand, mud and gravel that was most likely deposited in a lacustrine environment. Instead, we prefer a  
468 perspective where the pattern of residual gravity anomaly values reflects spatial variations in the  
469 thickness of the Quaternary sediments. Accordingly, the thickest Quaternary suite can be found  
470 upstream and downstream of Bern (Figure 5b), where the Aare main overdeepening is between 4 and 5  
471 km wide and >200 m deep, consistent with drilling information (Bandou et al., 2023). In the city area  
472 of Bern, however, the main trough tends to become shallower. This is indicated by the thickness of the  
473 Quaternary sediments reaching 100 m and possibly less (Figure 5b). The thickness of the Quaternary  
474 sediments filling the trough then increases again farther downstream.

475

#### 476 4.3 *The consideration of deep drillings discloses the occurrence of slot canyons*

477 The reconstructed bedrock topography of the target region reveals a complex pattern (Figure 6), which  
478 can be described as a bedrock riegel that is dissected by multiple, partly anastomosing slot canyons or  
479 inner gorges (Bandou et al., 2023). At this stage, we cannot precisely reconstruct the number of the  
480 inferred canyons because we lack a high-resolution database of deep drillings (Figure 6). Yet, the  
481 discrepancy between (i) a relatively low gravity signal particularly between the Wabern2 and the Bern  
482 sections (Figure 5a) and (ii) drillings that reached the bedrock at much deeper levels >200 m below the  
483 surface (Figures 6) can only be resolved by invoking the occurrence of a plateau at shallow elevations  
484 that is dissected by one or multiple slot canyons (Figure 7). These gorges are up to 150 m deep and may  
485 connect the overdeepened basins upstream and downstream of the city area of Bern. In particular, south  
486 of Bern along the Aare profile (Figures 2b and 8a), the Aare main overdeepening has a cross-section  
487 that displays two superimposed levels of U-shapes, each of which with steep lateral flanks and a flat

Deleted: .



489 base. While the upper flat base occurs at an elevation of c. 450 m a.s.l., the lower flat contact to the  
490 bedrock is situated at c. 250 m a.s.l. and thus approximately 200 m deeper than the upper level (Bandou  
491 et al., 2022). Approximately 5 km farther downstream along the Airport section (Figures 2b, 8b), the  
492 cross-sectional geometry of the Aare main overdeepening maintains its generally U-shaped geometry  
493 with a base at an elevation between 200 and 250 m a.s.l. There, the base of the overdeepening appears  
494 less flat than farther upstream, but we acknowledge that the density of deep drillings in the region  
495 (Figure 6) and the resolution of the gravity data (Figure 5a, Bandou et al., 2023) is not high enough to  
496 fully support this comparison. Upon approaching the city area of Bern, the base of the bedrock becomes  
497 shallower and appears to evolve towards a plateau particularly between the Kehrsatz and Bern2 sections  
498 (Figures 6, 7, 8c, d and e). This plateau is situated at an elevation of c. 400 m a.s.l. (dashed lines on  
499 Figure 8) and dissected by multiple slot-canyons, as evidenced by drillings reaching depths down to c.  
500 300 m a.s.l. and even lower elevations, yet the canyons remain undetected by the gravity survey. This  
501 implies that the canyons must be cutting up to 150 m deep below the plateau at c. 400 m a.s.l. and that  
502 they are too narrow to be detected by the gravity survey (Bandou et al., 2023). Farther to the Northwest  
503 reaching the terminal part of the Aare main overdeepening (Figure 2b), the trough widens again and  
504 gives way to a relatively deep basin where the deepest part occurs at an elevation of almost 300 m a.s.l.  
505 (Figures 6, 8f). This terminal basin appears to be connected with the Bümpliz tributary trough farther  
506 to the SW. Yet the density of drillings is too low (Figure 6) to determine whether a possible bedrock  
507 swell separates the Aare main overdeepening from the Bümpliz tributary trough (Figure 2b).

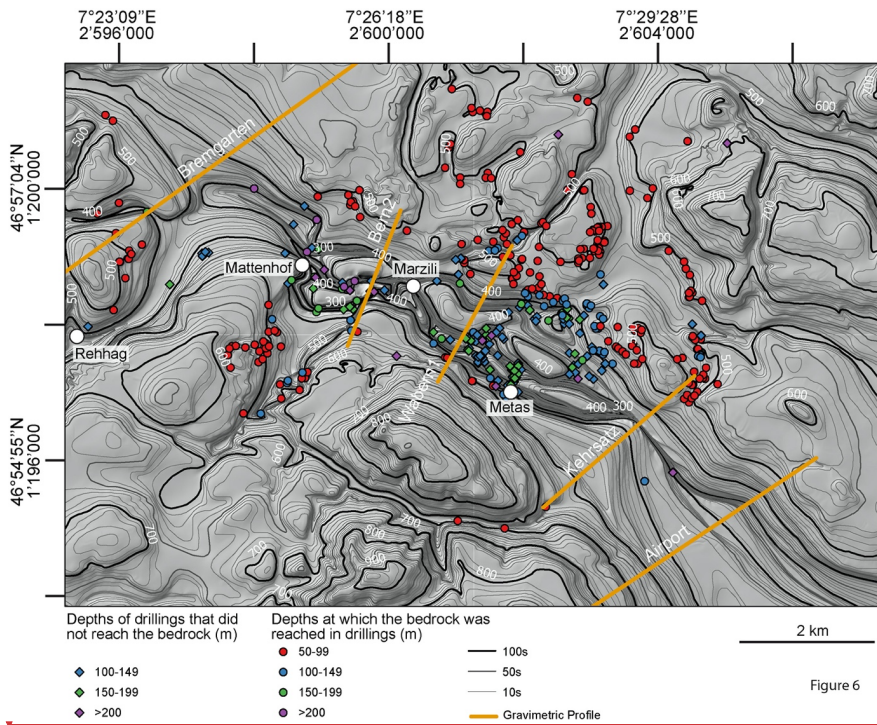
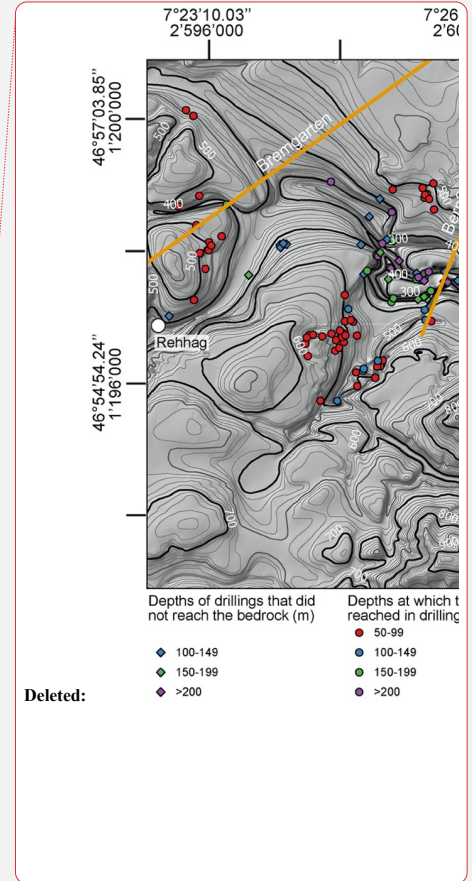


Figure 6: Hillshade DEM, illustrating the bedrock topography of the Bern area, together with deep drillings that either reached the bedrock (circles) or that ended in Quaternary sediments (diamonds). The shallow drillings (<50 m) are not displayed on this map since the number is too large (more than 1000, please see Reber and Schlunegger, 2016). The isohypses were drawn for every 10 m. The coordinates along the figure margin refer to the Swiss coordinate system (CH1903+). The sections shown on this map are used to illustrate the cross-sectional geometry of the overdeepening beneath Bern (see next figures). The white circles represent those drillings, the logs of which are illustrated in Figure 2d.



508

509

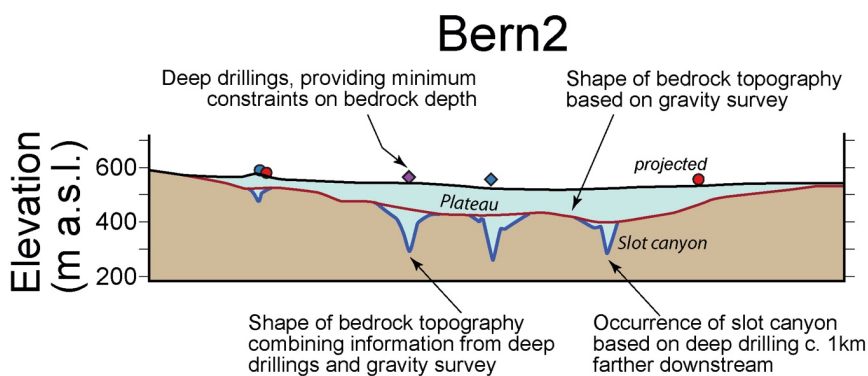


Figure 7

Figure 7: Example that illustrates how we proceeded upon reconstructing the bedrock topography beneath Bern. We started with the general shape of the bedrock topography using the gravity signal of the bulk Quaternary mass as a basis (red line, and Figure 5b). Information from drillings >50 m deep (circles and diamonds: see Figure 6 for explanation of colors) allowed then to reconstruct the course and geometry of the slot canyons (blue line). The mass of their Quaternary fill is too low to be identified by the gravity survey. This is the case because the strength of a gravity signal decays exponentially with depth (see also Bandou et al., 2023, for further explanations).

512

513

## 514 5 Discussion

### 515 5.1 Limitations upon reconstructing the bedrock topography model

516 The inferred existence of a bedrock riegel and slot canyons below Bern is based on two features: (i)  
 517 gravimetric data showing a relatively low negative anomaly, which we interpret as a low depth to  
 518 bedrock in the Bern city area, and (ii) previous borehole logs that show a much greater drilled depth to  
 519 bedrock. Indeed, the combination of deep bedrock detected from borehole data in an area of otherwise  
 520 characterized by shallow bedrock, as imaged by gravimetry, suggests that the canyons must extend  
 521 deeply while remaining highly confined in order to stay below the spatial resolution of the gravimetry  
 522 method. However, we acknowledge that no direct drilling evidence confirms the presence of such a  
 523 riegel. Nevertheless, the contour lines of the Bouguer anomaly values, calculated using a density of  
 524 bedrock ( $2500 \text{ kg/m}^3$ ), indicate that the target overdeepening is generally broad and deep upstream of  
 525 Bern, shallow beneath the city, and then narrows and deepens downstream of it (Figure 4). In addition,  
 526 gravity data collected at 10 gravity stations along the Bern2 profile does point towards the occurrence  
 527 of a residual anomaly signal with a short wavelength beneath the main large-wavelength residual gravity  
 528 anomaly (Figures S1a and S1b in the Supplement). Indeed, using the results of 3D gravity modelling,  
 529 Bandou et al. (2023) considered the large-wavelength anomaly to be the gravity response of the  
 530 Quaternary fill overlying the bedrock riegel, whereas the short-wavelength anomaly beneath it suggests  
 531 the possible presence of a slot canyon, filled by Quaternary sediments (Figure S1c in the Supplement).

Deleted: relatively

Formatted: English (UK)

Deleted: anomaly with the

Deleted:

Deleted: as

Formatted: English (UK)

Formatted: English (UK)

Formatted: English (UK)

Deleted: illustrates

Formatted: English (UK)

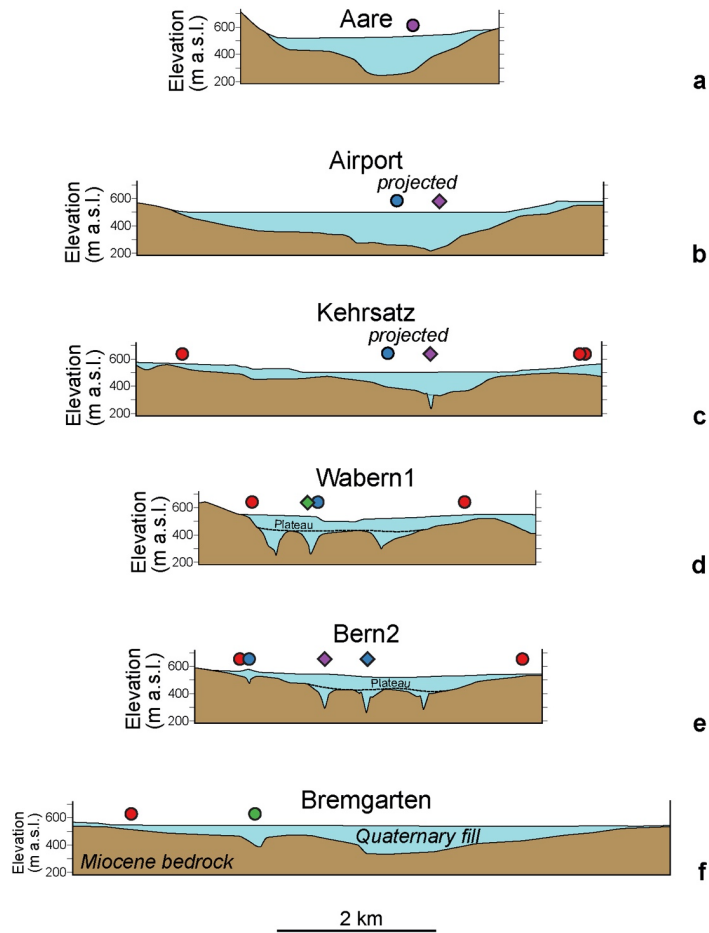
Deleted: occurrence

Deleted: ,

Formatted: English (UK)

Formatted: English (UK)

539 Further slot canyons could not be identified upon modelling due to a lack of resolution of the gravimetric  
 540 data.



<p>Depths of drillings that did not reach the bedrock (m)</p> <ul style="list-style-type: none"> <li>◆ 100-149</li> <li>◆ 150-199</li> <li>◆ &gt;200</li> </ul>	<p>Depths at which the bedrock was reached in drillings (m)</p> <ul style="list-style-type: none"> <li>● 50-99</li> <li>● 100-149</li> <li>● 150-199</li> <li>● &gt;200</li> </ul>
---	--

Figure 8

Figure 8: Sections through the Bern area, where the geometry of the bedrock is taken from the DEM illustrated in Figure 6. The Aare section is taken from Bandou et al. (2022). See Figures 2 and 6 for location and orientation of sections.

541

542

543 In summary, we are confronted with the situation that there is most likely a bedrock riegel imaged by  
544 the gravity data, and that thick Quaternary deposits (deep erosion) have been encountered in some deep  
545 drillings as well (and have also been detected in the Bern2 gravity profile; Figures S1a to S1b in the  
546 Supplement). We thus propose an interpretation where a bedrock riegel is cut by narrow slot canyons  
547 filled with Quaternary sediments, as such a scenario adequately combines the findings from our gravity  
548 survey and drilling information. Furthermore, using the modern examples such as the Aare gorge  
549 displayed on Figure 3a as a basis, we interpret that these slot canyons formed the hydrological link  
550 between the upstream and downstream basins. We exclude an alternative interpretation where the drilled  
551 Quaternary sequences represent the filling of isolated glacial potholes. Indeed, the short distance  
552 between the individual boreholes with thick Quaternary sequences and the almost linear arrangement  
553 of these boreholes, particularly near Wabern1 (Figure 6), suggests that the drilled sequences comprise  
554 the fill of continuous channels rather than potholes.

Formatted: English (UK)

## 555 5.2 Subglacial origin and the role of subglacial meltwater

556 It is agreed upon in the literature that the formation of overdeepened basins can be understood as the  
557 response of erosion by glaciers. The main arguments that have been put forward are (i) the depths of  
558 the base of these depressions, which are generally below the current fluvial base-level, and (ii) the  
559 occurrence of adverse slopes in the downstream direction of these basins (Figure 1, Preusser et al., 2010;  
560 Patton et al., 2016; Alley et al., 2019; Magrani et al., 2022; Gegg and Preusser, 2023). Such geometric  
561 features are also encountered for the Aare main overdeepening beneath the city area of Bern. Therefore,  
562 the origin of this depression has repeatedly been interpreted as the response of the erosional processes  
563 of a glacier with a source in the Central Alps of Switzerland (Dürst Stucki et al., 2010; Preusser et al.,  
564 2010; Reber and Schlunegger, 2016; Magrani et al., 2022; Bandou et al., 2023). As a refinement already  
565 outlined by Bandou et al. (2023) and further detailed in this work, the overdeepening beneath Bern can  
566 be subdivided into a southeastern and a northwestern sub-basin. These depressions are separated by a  
567 bedrock riegel or swell, which itself is dissected by one or multiple slot canyons establishing a  
568 hydrological link between the upstream and downstream basins (Figure 6). Such ensembles of basins,  
569 riegels and slot canyons (or inner gorges) are common features in Alpine valleys (Figure 3) and have  
570 therefore been the target of previous research. In this context, it was proposed that such gorges and  
571 riegels in the Alps were likely shaped during several glacial/interglacial periods (Montgomery and  
572 Korup, 2011), and that the incision of the canyons occurred during the decay of glaciers and ice caps,  
573 when large volumes of meltwater were released (Steinemann et al., 2021). As further, yet only partly  
574 related examples, erosion by subglacial meltwater was put forward to explain the formation of inner  
575 gorges at the margin of the Fennoscandian ice sheet (based on the pattern of surface exposure ages;  
576 Jansen et al., 2014), and such a mechanism was used to explain (i) the origin of the deep channels on  
577 the floor of the eastern English Channel, and (ii) the breaching of the bedrock swell at the Dover strait  
578 during the aftermath of the Marine Isotope Stage (MIS) 12 or a later glaciation (Gupta et al., 2007;  
579

Formatted: English (UK)

Formatted: English (UK)

Formatted: English (UK)

Formatted: English (UK)

580 Cohen et al., 2014; Gupta et al., 2017). In this context, Jansen et al. (2014) noted that typical field  
581 evidence for inferring a subglacial meltwater control includes (i) the occurrence of anastomosing  
582 channels, (ii) undulating valley long profiles, and (iii) a topography that apparently amplifies the  
583 hydraulic potential. The resolution of our data is not enough to see such details of the valley long  
584 profiles, but sufficient to display the anastomosing patterns of the slot canyons, with channels  
585 meandering, splitting and merging again (Figure 6).

Formatted: English (UK)

### 587 5.3 *Formation through erosion by subglacial meltwater inferred from theory and modelling*

588 Besides the geometrical arguments and field-based observations outlined in the previous section, a  
589 subglacial meltwater influence on the formation of overdeepenings has also been inferred based on  
590 theoretical considerations, including the relationships between meltwater runoff and the sediment  
591 transport capacity of proglacial and subglacial streams (e.g., Boulton and Hindmarsh, 1987; Alley et  
592 al., 1997; Herman et al., 2011, Beaud et al., 2016). Because sediment transport increases exponentially  
593 with both the volume and seasonality of meltwater runoff, Alley et al. (1997) interpreted that subglacial  
594 and proglacial streams are among the most efficient sediment-transport mechanisms on Earth. This  
595 process peaks in the ablation zone of a glacier, where surface melt reaches the bed and significantly  
596 contributes to the generation of subglacial runoff. Also on theoretical grounds, Cohen et al. (2023)  
597 showed that subglacial meltwater is able to remove the sediment from the base of a glacier and to further  
598 incise into bedrock provided that the pressure of the subglacial meltwater and that of the ice overburden  
599 are at least the same (Boulton and Hindmarsh, 1987). The results from the model of Cohen et al. (2023),  
600 tailored to determine the location of the subglacial drainage pathways, further suggest that such  
601 conditions most likely prevailed at the front of piedmont glaciers and particularly during the decaying  
602 stage of a glacier when large volumes of meltwater were available. In addition, the model predicts that  
603 under such circumstances, the locations of subglacial meltwater pathways are likely to coincide with  
604 segments where high rates of glacial erosion occur (Cohen et al., 2023). Therefore, reaches with  
605 evidence for intense erosion by both water and ice occur in the same area and are hydrologically  
606 connected with each other. We propose this to be the case for the ensemble of overdeepened basins and  
607 slot canyons beneath Bern.

Formatted: English (UK)

Formatted: English (UK)

Formatted: English (UK)

### 609 5.4 *The role of bedrock strength and the confluence of two glaciers*

610 The formation of riegels and basins is consensually understood as conditioned by differences in bedrock  
611 strengths. This also concerns the controls on the size of a basin itself where bedrock with a high  
612 erodibility tends to host a larger basin than lithologies where the erodibility is low (e.g., Magrani et al.,  
613 2020; Gegg and Preusser, 2023). Following this logic, swells preferentially would form in locations  
614 where the bedrock has a lower erodibility than the rock units farther upstream and downstream. This  
615 has been documented for the riegel in the Aare valley, which separates an overdeepened basin upstream

616 from a wide valley farther downstream (Figure 3a). There, the bedrock riegel is made up of the Quinten  
617 Formation (Gisler et al., 2020; Stäger et al., 2020). These limestones tend to have a lower erodibility  
618 (Kühni and Pfiffner, 2001) than the sandstone-marl alternations (North Helvetic Flysch; Gisler et al.,  
619 2020; Stäger et al., 2020) downstream of the bedrock swell, and the suite of sandstones, marls and  
620 dolomite beds upstream of it (Mels- and Quarten Formations; Gisler et al., 2020; Stäger et al., 2020).  
621 Another example is offered by the riegel in the Trift valley (Figure 3b), where the bedrock forming the  
622 ridge is made up of a banded, biotite-rich gneiss (Erstfeld gneiss). Upstream and downstream of the  
623 swell, the bedrock is cut by multiple faults and fractures, thus offering a lower resistance to erosion  
624 (Steinemann et al., 2021). In the Bern area, the bedrock architecture is comparable to the examples  
625 explained above where the UMM, which has a low erodibility, forms the swell, whereas the LFM with  
626 a relatively large erodibility constitutes the bedrock downstream of the riegel (section 2.3). In addition,  
627 the NW-SE striking faults in the Molasse bedrock (Isenschmid, 2019), which offer zones of mechanical  
628 weaknesses, most likely controlled the course of the slot canyons as they have the same orientation.  
629 Presumably as important as the contrasts in bedrock erodibility: the bedrock swell underneath Bern is  
630 situated in the confluence area between the Valais and Aare glaciers (Figure 2b). The occurrence of  
631 swells at the confluence ~~area~~ is consistent with observations in Alpine valleys (Figure 3) and with  
632 topographic and bathymetric DEMs of overdeepenings in Labrador, Canada (Lloyd et al., 2023). In this  
633 case, the deep carving into the bedrock would be the result of an acceleration of the ice flow (Herman  
634 et al., 2015) in response to the increase in the ice flux downstream of the confluence region.  
635 Alternatively, a bedrock riegel could also form upstream of the confluence of two glaciers (see e.g., the  
636 Maggia valley as modern example, Figure 3c). For the Bern area, the damming of the Aare glacier by  
637 the much larger Valais glacier could have caused a reduction of the flow velocity of the Aare glacier  
638 (Figure 2b). Consequently, the shear velocity and thus the bedrock abrasion rates would decrease,  
639 thereby facilitating the preservation of a bedrock swell.

Deleted: areas

#### 641 5.5 Differences in the geometries between the exposed riegels and basins in Alpine valleys, and the 642 overdeepening beneath Bern

643 Despite obvious similarities between the geometric properties of the overdeepening system beneath  
644 Bern and the currently exposed riegels and slot canyons in Alpine valleys, there are also major  
645 differences (Figure 3 versus Figures 6 and 8). The most striking one is the occurrence, beneath Bern, of  
646 the riegel and inner gorges approximately 50-100 m below the current base-level, and the absence of  
647 an obvious continuation of the thalweg NW of Bern (Figure 2c). Accordingly, the inferred interpretation  
648 where the slot canyons beneath Bern were formed by subglacial meltwater requires a mechanism where  
649 the meltwater is not only capable to incise into bedrock beneath a glacier, but also to escape the  
650 depression by ascending nearly 200 m from the base of the overdeepening to the surface near the  
651 glacier's snout. Using Bernoulli's principle as a basis (e.g., Batchelor, 1967), it was proposed that such

653 an ascent of subglacial meltwater was driven by the translation of high hydrostatic pressure into  
654 hydrodynamic pressures at the downstream margin of a glacier (Dürst Stucki and Schlunegger, 2013).  
655 Such a mechanism is most effective at work where the surface slope of a glacier is steeper than the  
656 adverse slope of an overdeepening (Hooke and Pohjola, 1994), as is commonly found in the frontal part  
657 of a glacier (Figure 1a). Since the ratio between the densities of ice and water is  $>0.9$  (Harvey, 2019),  
658 the inferred 200 m-rise of the meltwater requires a minimum hydrostatic pressure corresponding to  
659  $>220$  m-thick ice to allow an upward water flow. Such a scenario is plausible, as the Aare glacier in the  
660 Bern area was estimated to have reached several hundred meters in thickness during past glaciations  
661 (Bini et al., 2009; Preusser et al., 2011; Figure 2b). If this hypothesis is valid, then the thickness of the  
662 piedmont glaciers sets an uppermost limit to the depth at which overdeepenings can be carved into the  
663 bedrock, since it represents the driver of overpressure required for the subglacial meltwater to ascend  
664 to the surface from deeper levels.

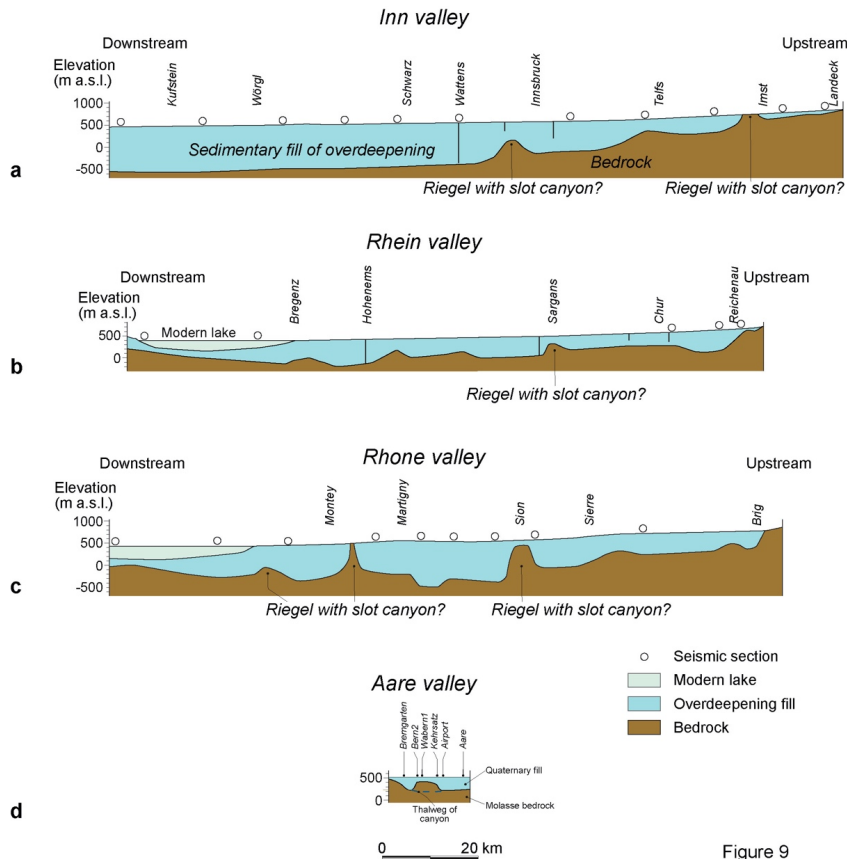
665

## 666 **6 Conclusions**

667 Bedrock riegels separating upstream and downstream basins are common features in modern Alpine  
668 valleys, and they have been documented from overdeepenings in the region of Bern. We propose that  
669 these riegels occur as ensembles together with slot canyons that cut through these swells and establish  
670 a hydrological link between the upstream and downstream basins. We suggest this based on our  
671 reconstruction of the bedrock topography of the Aare main overdeepening in the Bern area, and we  
672 propose that such ensembles of basins, riegels and slot canyons also occur in other Alpine  
673 overdeepenings such as the Rhone, Rhine and Inn valleys (Figure 9). We further suggest that these slot  
674 canyons were formed through incision by glacial meltwater during the deglaciation when large volumes  
675 of meltwater were available. As the flow must counteract adverse slopes, it may also be envisioned that  
676 the slot canyons formed during glacial maxima, when ice thickness (and thus excess hydrostatic  
677 pressure) is maximum, driving vigorous underflows. For the bedrock swell underneath Bern, the  
678 resolution of the dataset presented in this work does not allow to locate and reconstruct the precise  
679 course of the inferred slot canyons. However, the presented reconstruction of the bedrock topography  
680 reconciles (i) the occurrence of low residual gravity anomalies in the Bern area (Figure 5a), which  
681 suggests a topographic high of the incised bedrock marking the base of the overdeepening, and (ii) the  
682 significant depth at which Quaternary sediments were encountered in drillings, indicating deep-reaching  
683 bedrock incision (Figures 6, 7). In many Alpine valleys, such ensembles of riegel and slot canyons  
684 appear to be preferentially formed in the confluence area between two glacial valleys and where the  
685 bedrock has a relatively low erodibility. We posit that this configuration is also valid for the  
686 overdeepening below the Bern area, where such a bedrock swell appears to be situated just upstream of  
687 the confluence between the Aare and Valais glaciers, at least during LGM times and possibly during



688 previous glaciations. In addition, the inferred bedrock riegel beneath Bern is located where the bedrock  
 689 has a lower erodibility than farther downstream.



690 Figure 9

691 Figure 9: Sections showing the patterns of overdeepenings from upstream to downstream for a) the Inn  
 692 valley, b) the Rhine valley, c) the Rhone valley and d) the Aare valley in the Bern area. The  
 693 examples of the Inn, the Rhine and the Rhone valleys are taken from Hinderer (2001), whereas  
 694 the section along the Aare valley is a modified version of Bandou et al. (2023) and bases on the  
 695 data presented in Figure 6. The data from the Aare valley covers a short distance only, but it shows  
 696 a striking similarity to the riegels in the large Alpine valleys. Therefore, it is quite likely that the  
 697 other riegels are also dissected by narrow channels and that all settings share a similar origin.

698 In summary, we present a bedrock model that documents an upstream-downstream trend of the  
 699 subglacial drainage network: (i) Along the Aare cross-section, which is situated upstream of the riegel  
 700 there appears to be no evidence of a channelised subglacial drainage network incising into the bedrock;  
 701 (ii) in the area of the inferred riegel, we postulate the occurrence of an anastomosing network of slot  
 702 canyons based on drilling information, which evolves (iii) downstream of the riegel into a single canyon  
 703 as seen along the Bremgarten cross-profile. This rises further questions about the mechanisms that could

698 be responsible for these changes in the network, how such processes evolved in space and time, and  
699 how possible variations in the subglacial drainage network would have affected bedrock erosion and  
700 ice flow. Answers to such following up questions require detailed constraints on the ages and the  
701 sedimentary architecture of the Quaternary fill, which are not available. Yet, the few chronological  
702 information published on the Quaternary fill of overdeepenings in the Swiss Plateau does support an  
703 interpretation where the deep carving occurred during multiple stages since the Middle Pleistocene  
704 Transition c. 800 ka ago (Schlüchter, 2004). Apparently, the change in the frequency of glacial-  
705 interglacial cycles from a 40 ka- to a 100 ka-periodicity, which occurred at that time, not only resulted  
706 in rapid glacial erosion (Pedersen and Egholm, 2013) and in the deep glacial carving of U-shaped  
707 valleys in the Alps (Häuselmann et al., 2007, Valla et al., 2011), but also in the formation of  
708 overdeepenings with complex geometries including basins, riegels and slot canyons in the foreland.

709

710

#### 711 **Acknowledgement**

712 This work was financially supported by the Swiss National Science Foundation (project No.  
713 200021\_175555) with contributions from the Stiftung Landschaft und Kies, swisstopo and the  
714 Gebäudeversicherung Bern GVB.

715

#### 716 **Data availability**

717 All data used in this paper can be ordered by the Authorities of the Canton Bern and by the authors on  
718 request.

719

#### 720 **Author contributions**

721 EK designed the study, together with FS and DB. DB collected the gravity data and processed them,  
722 with support by UM and EK. FS wrote the paper and conducted the analyses and interpretation of the  
723 data. RR drafted the bedrock topography map. PS, MS, DM and GD contributed to the discussion. All  
724 authors approved the article.

725

#### 726 **Competing interests**

727 The authors declare that they have no conflict of interest.

728

#### 729 **References**

730 Alley, R.B., Cuffey, K.M., Evenson, E.B., Strasser, J.C., Lawson, D.E., and Larson, G.J.: How glaciers  
731 entrain and transport basal sediment: physical constraints. *Quat. Sci. Rev.*, 16, 1017-1038, 1997.

732 Alley, R., Cuffey, K., and Zoet, L.: Glacial erosion: Status and outlook. *Ann. Glaciol.*, 60, 1–13,

733 <https://doi.org/10.1017/aog.2019.38>, 2019.

Field Code Changed

734 Anderson, R.S., Molnar, P., and Kessler, M.A.: Features of glacial valley profiles simply explained. *J.*  
735 *Geophys. Res., Earth Surface*, 111, F01004, doi:10.1029/2005JF000344, 2006.

736 Anselmetti, F., Bavec, M., Crouzet, C., Fiebig, M., Gabriel, G., Preusser, F., Ravazzi, C., and Dove  
737 team.: Drilling Overdeepened Alpine Valleys (ICDP-DOVE): quantifying the age, extent, and  
738 environmental impact of Alpine glaciations. *Sci. Drill.*, 31, 51–70, [https://doi.org/10.5194/sd-](https://doi.org/10.5194/sd-31-51-2022)  
739 31-51-2022, 2022.

740 Bandou, D.: Overdeepenings in the Bern region, Switzerland: Understanding their formation processes  
741 using 3D gravity forward modelling. PhD thesis, univ. Bern, Switzerland, 381pp,  
742 <https://boristheses.unibe.ch/id/eprint/4573>, 2023a.

743 Bandou, D.: Gravi3D: A 3D forward modelling software using gravity data to resolve the geometry of  
744 subsurface objects. <https://zenodo.org/doi/10.5281/zenodo.8153258>, 2023b.

745 Bandou, D., Schlunegger, F., Kissling, E., Marti, U., Schwenk, M., Schläfli, P., Douillet, G., and Mair,  
746 D.: Three-dimensional gravity modelling of a Quaternary overdeepening fill in the Bern area of  
747 Switzerland discloses two stages of glacial carving. *Scientific Rep.*, 12, 1441,  
748 <https://doi.org/10.1038/s41598-022-04830-x>, 2022.

749 Bandou, D., Schlunegger, F., Kissling, E., Marti, U., Reber, R., and Pfander J.: Overdeepenings in the  
750 Swiss plateau: U-shaped geometries underlain by inner gorges. *Swiss. J. Geosci.*, 116, 19,  
751 <https://doi.org/10.1186/s00015-023-00447-y>, 2023.

752 Banerjee, B., and Das Gupta, S.P.: Gravitational attraction of a rectangular parallelepiped. *Geophysics*,  
753 42, 1053–1055, 1977.

754 Batchelor, G. K.: An introduction to fluid dynamics (p. 615). Cambridge Univ. Press, 1967.

755 Beaud, F., Flowers, G.E., and Venditti, J.G.: Efficacy of bedrock erosion by subglacial water flow. *Earth*  
756 *Surf. Dyn.*, 4, 125-145, <https://doi.org/10.5194/esurf-4-125-2016>, 2016.

757 Bini, A., et al.: Die Schweiz während des letzteiszeitlichen Maximums (LGM) 1:500'000. Bundesamt  
758 für Landestopografie swisstopo, Bern, Switzerland, 2009.

759 Boulton, G.S., and Hindmarsh, R.C.A.: Sediment deformation beneath glaciers: rheology and  
760 geological consequences. *J. Geophys. Res.* 92, 9059-9082, 1987.

761 Brocklehurst, S.H., and Whipple, K.X.: Glacial erosion and relief production in the eastern Sierra  
762 Nevada, California. *Geomorphology* 42, 1–24, 2002.

763 Brocklehurst, S.H., Whipple, K.X., and Foster, D.: Ice thickness and topographic relief in glaciated  
764 landscapes of the western USA. *Geomorphology*, 97, 35-51,  
765 <https://doi.org/10.1016/j.geomorph.2007.02.037>, 2008.

766 Büchi, M. W., Frank, S. M., Graf, H. R., Menzies, J., and Anselmetti, F. S.: Subglacial emplacement of  
767 tills and meltwater deposits at the base of overdeepened bedrock troughs. *Sedimentology*, 64,  
768 685, <https://doi.org/10.1111/sed.12319>, 2017.

Field Code Changed

Formatted: English (UK)

Formatted: English (UK)

Formatted: English (UK)

Formatted: English (UK)

Field Code Changed

Field Code Changed

Field Code Changed

Field Code Changed

Formatted: English (UK)

Formatted: English (UK)

Field Code Changed

Field Code Changed

769 Büchi, M., Graf, H.R., Haldimann, P., Lowick, S.E. and Anselmetti, F.S.: Multiple Quaternary erosion  
770 and infill cycles in overdeepened basins of the northern Alpine foreland. *Swiss J. Geosci.*, 111,  
771 133-167, <https://doi.org/10.1007/s00015-017-0289-9>, 2018.

772 Burschil, T., Bunes, H., Tanner, D.C., Wiedlandt-Schuster, U., Ellwanger, D., and Gabriel, G.: High-  
773 resolution reflection seismics reveal the structure and the evolution of the Quaternary glacial  
774 Tannwald Basin. *Near Surf. Geophys.*, 16, 593-610, <https://doi.org/10.1002/nsg.12011>, 2018.

775 Burschil, T., Tanner, D., Reitner, J., Bunes, H., and Gabriel, G.: Unravelling the complex stratigraphy  
776 of an overdeepened valley with high-resolution reflection seismics: The Lienz Basin (Austria),  
777 *Swiss J. Geosci.*, 112, 341–355, <https://doi.org/10.1007/s00015-019-00339-0>, 2019.

778 Clark, P.U., and Walder, J.S. Subglacial drainage, eskers, and deforming beds beneath the Laurentide  
779 and Eurasian ice sheets. *Geol. Soc. Amer. Bull.*, 106, 304-314, [https://doi.org/10.1130/0016-7606\(1994\)106<0304:SDEADB>2.3.CO;2](https://doi.org/10.1130/0016-7606(1994)106<0304:SDEADB>2.3.CO;2), 1994.

781 Cohen, K. M., Gibbard, P. L., and Weerts, H. J. T.: North Sea palaeogeographical reconstructions for  
782 the last 1 Ma. *Neth. J. Geosci.* 93, 7–29, 2014.

783 Cohen, D., Juvet, G., Zwinger, T., Landgraf, A., and Fischer, U.H.: Subglacial hydrology from high-  
784 resolution ice-flow simulations of the Rhine Glacier during the Last Glacial Maximum: a proxy  
785 for glacial erosion. *E&G Quat. Sci. J.*, 72, 189-201, <https://doi.org/10.5194/egqsj-72-189-201>,  
786 2023.

787 Cook, S. J., and Swift, D. A.: Subglacial basins: Their origin and importance in glacial systems and  
788 landscapes. *Earth-Science Rev.*, 115, 332–372,  
789 <https://doi.org/10.1016/j.earscirev.2012.09.009>, 2012.

790 Dehnert, A., Lowick, S.E., Preusser, F., Anselmetti, F.S., Drescher-Schneider, R., Graf, H.R., Heller,  
791 F., Horstmeyer, H., Kemna, H.A., Nowaczyk, N.R., Züger, and Furrer, H.: Evolution of an  
792 overdeepened trough in the northern Alpine Foreland at Niederweningen, Switzerland. *Quat.*  
793 *Sci. Rev.*, 34, 127-145, <https://doi.org/10.1016/j.quascirev.2011.12.015>, 2012.

794 Dietrich, P., Griffis, N. P., Le Heron, D. P., Montañez, I. P., Kettler, C., Robin, C., and Guillocheau, F.:  
795 Fjord network in Namibia: A snapshot into the dynamics of the late Paleozoic glaciation.  
796 *Geology*, 49, 1521-1526, <https://doi.org/10.1130/G49067.1>, 2021.

797 Douillet, G., Ghienne, J. F., Géraud, Y., Abueladas, A., Diraison, M., and Al-Zoubi, A.: Late Ordovician  
798 tunnel valleys in southern Jordan. *Geol. Soc. London Spec. Publ.*, 368, 275-292,  
799 <https://doi.org/10.1144/sp368.4>, 2012.

800 Dürst Stucki, M., Reber, R., and Schlunegger, F.: Subglacial tunnel valleys in the Alpine foreland: An  
801 example from Bern, Switzerland. *Swiss J. Geosci.*, 103, 363–374,  
802 <https://doi.org/10.1007/s00015-010-0042-0>, 2010.

Field Code Changed

Field Code Changed

Field Code Changed

Field Code Changed

Field Code Changed

Field Code Changed

Field Code Changed

Field Code Changed

Field Code Changed

803 Dürst-Stucki, M., and Schlunegger, F.: Identification of erosional mechanisms during past glaciations  
804 based on a bedrock surface model of the central European Alps. *Earth Planet. Sci. Lett.*, 384,  
805 57–70. <https://doi.org/10.1016/j.epsl.2013.10.009>, 2013.

806 Egholm, D.L., Nielsen, S., Pedersen, V., and Lesemann, J.: Glacial effects limiting mountain height.  
807 *Nature*, 460, 884–887, <https://doi.org/10.1038/nature08264>, 2009.

808 Feiger, N., Huss, M., Leinss, S., Sold, L., and Farinotti, D.: The bedrock topography of Gries- and  
809 Findelengletscher. *Geogr. Helv.*, 73, 1–9, <https://doi.org/10.5194/gh-73-1-2018>, 2018.

810 Fischer, U., and Häberli, W.: Overdeepenings in glacial systems: Processes and uncertainties. *Eos*, 93,  
811 35, 341–341, <https://doi.org/10.1029/2012EQ0350010>, 2012.

812 Garefalakis, P., and Schlunegger, F.: Tectonic processes, variations in sediment flux, and eustatic sea  
813 level recorded by the 20 Myr old Burdigalian transgression in the Swiss Molasse basin. *Solid*  
814 *Earth*, 10, 2045–2972, <https://doi.org/10.5194/se-10.2045-2019>, 2019.

815 Gees: Spühlbohrung Bern B1. *Wasser und Energiewirtschaft des Kantons Bern*, 1974.

816 Gegg, L., Deplazes, G., Keller, L., Madritsch, H., Spillmann, T., Anselmetti, F. S., and Büchi, M.W.:  
817 3D morphology of a glacially overdeepened trough controlled by underlying bedrock geology.  
818 *Geomorphology*, 394, 107950, <https://doi.org/10.1016/j.geomorph.2021.107950>, 2021.

819 Gegg, L., and Preusser, F.: Comparison of overdeepened structures in formerly glaciated areas of the  
820 northern Alpine foreland and northern central Europa. *E&G Quat. Sci. J.*, 72, 23–36,  
821 <https://doi.org/10.5194/egqsj-72-23-2023>, 2023.

822 Geotest: Grundlagen für Schutz und Bewirtschaftung der Grundwasser des Kantons Bern.  
823 Hydrogeologie Gürbetal und Stockental. *Wasser- und Energiewirtschaftsamt des Kantons Bern*  
824 WEA, 123 pp, 1995.

825 Geotest: Kernbohrung Kb 97.1. *Wasser und Energiewirtschaft des Kantons Bern WEA*, 1997.

826 [Geotest: Erdsonde Bern, Munzingenstr. 11, ES 2. Amt für Wasser und Abfall des Kantons Bern AWA,](#)  
827 [2013.](#)

828 Gerber, E.: *Geologische Karte von Bern und Umgebung 1:25'000*. Kümmerli und Frei, Bern, 1927.

829 Gisler, C., Labhart, T., Spillmann, P., Herwegh, M., Della Valla, G., Trüssel, M., and Wiederkehr, M.:  
830 Erläuterungen. *Geologischer Atlas der Schweiz 1:25'000, 1210 Innertkirchen, Schweiz. Geol.*  
831 *Komm.*, 2020.

832 Gupta, S., Collier, J.S., Palmer-Felgate, A., and Potter, G.: Catastrophic flooding origin of shelf valley  
833 systems in the English Channel. *Nature*, 448, 342–345, <https://doi.org/10.1038/nature06018>,  
834 2007.

835 Gupta, S., Collier, J. S., Garcia-Moreno, D., Oggioni, F., Trentesaux, A., Vanneste, K., De Batist, M.,  
836 Camelbeeck, T., Potter, G., Van Vliet-Lanoë, B., and Arthur, J. C. R.: Two-stage opening of  
837 the Dover Strait and the origin of island Britain. *Nat. Comm.*, 8, 15101,  
838 <https://doi.org/10.1038/ncomms15101>, 2017.

Field Code Changed

Field Code Changed

Formatted: English (UK)

Formatted: English (UK)

Formatted: English (UK)

Formatted: English (UK)

Field Code Changed

Field Code Changed

Field Code Changed

Field Code Changed

Formatted: English (UK)

Field Code Changed

Field Code Changed

839 Häberli, W., Linsbauer, A., Cochachin, A., Salazar, C., and Fischer, U.H.: On the morphological  
840 characteristics of overdeepenings in high-mountain glacier beds. *Earth Surf. Proc. Landf.*, 41,  
841 1980–1990, <https://doi.org/10.1002/esp.396>, 2016.

842 Hantke, R., and Scheidegger, A. E.: Zur Genese der Aareschlucht (Berner Oberland, Schweiz). *Geogr.*  
843 *Helv.*, 48, 120–124, <https://doi.org/10.5194/gh-48-120-1993>, 1993.

844 Harvey, A. H.: Properties of Ice and Supercooled Water, in: *CRC Handbook of Chemistry and Physics*  
845 (97th ed.), edited by Haynes, W. Lide, D. R. and Bruno, T., Boca Raton, FL: CRC Press., 2019.

846 Häuselmann, P., Granger, D.E., Jeannin, P.-Y., and Lauritzen, S.-E.: Abrupt glacial valley incision at  
847 0.8 Ma dated from cave deposits in Switzerland. *Geology*, 35, 143–146,  
848 <https://doi.org/10.1130/G23094A>, 2007.

849 Herman, F., and Braun, J.: Evolution of the glacial landscape of the Southern Alps of New Zealand:  
850 insights from a glacial erosion model. *J. Geophys. Res.* 113, F02009,  
851 <https://doi.org/10.1029/2007JF000807>, 2008.

852 Herman, F., Beaud, F., Champagnac, J.-D., Lemiux, J.-M., and Sternai, P.: Glacial hydrology and  
853 erosion patterns: a mechanism for carving glacial valleys. *Earth Planet. Sci. Lett.* 310, 498–508,  
854 <https://doi.org/10.1016/j.epsl.2011.08.022>, 2011.

855 Herman, F., Beyssac, O., Brughelli, M., Lane, S.N., Leprince, S., Adatte, T., Lin, J.Y.Y., Avouac, J.-  
856 P., and Cox, S.C.: Erosion by an Alpine glacier. *Science*, 350, 193–195,  
857 <https://doi.org/10.1126/science.aab2386>, 2015.

858 Hinderer, M. Late Quaternary denudation of the Alps, valley and lake fillings and modern river loads.  
859 *Geodinamica Acta*, 14, 231–263, <https://doi.org/10.1080/09853111.2001.11432446>, 2001.

860 Hooke, R.L., and Pohjola, V.A.: Hydrology of a segment of a glacier situated in an overdeepening,  
861 Storglaciären, Sweden. *J. Glaciol.*, 40, 140–148, <https://doi.org/10.3189/S002214300003919>,  
862 1994.

863 Isenschmid, C.: Die Grenze Untere Süswassermolasse/Obere Meeremolasse als Schlüssel zur Tektonik  
864 in der Region Bern. *Mitt. Natf. Ges. Bern*, 76, 108–133, 2019.

865 Jansen, J.D., Codilean, A.T., Stroeve, A.P., Fabel, D., Hättstrand, C., Kleman, J., Harbor, J.M.,  
866 Heyman, J., Kubik, P.W., and Xu, S.: Inner gorges cut by subglacial meltwater during  
867 Fennoscandian ice sheet decay. *Nat. Comm.*, 5, 3815, <https://doi.org/10.1038/ncomms4815>,  
868 2014.

869 Jørgensen, F., and Sandersen, P.B.E.: Buried and open tunnel valleys in Denmark—erosion beneath  
870 multiple ice sheets. *Quat. Sci. Rev.*, 25, 1339–1363,  
871 <https://doi.org/10.1016/j.quascirev.2005.11.006>, 2006.

872 Jordan, P.: Analysis of overdeepened valleys using the digital elevation model of the bedrock surface  
873 of northern Switzerland. *Swiss J. Geosci.*, 103, 375–384, <https://doi.org/10.1007/s00015-010-0043-z>,  
874 2010.

Formatted: English (UK)

Field Code Changed

Field Code Changed

Field Code Changed

Field Code Changed

Field Code Changed

Field Code Changed

Formatted: English (UK)

Field Code Changed

Field Code Changed

Field Code Changed

875 Kehew, A.E., Piotrowski, J.A., and Jørgensen, F.: Tunnel valleys: concepts and controversies – a  
876 review. *Earth-Sci. Rev.* 113, 33–58, <https://doi.org/10.1016/j.earscirev.2012.02.002>, 2012.

877 Kellerhals, P., and Häfeli, C.: Brunnenbohrung Münsingen. Geologische Dokumentation des Kantons  
878 Bern, WEA-Geologie, Beilage Nr. 2, 7 pp, 1984.

879 Kissling, E., Schwendener, H.: The Quaternary sedimentary fill of some Alpine valleys by gravity  
880 modeling. *Eclogae Geol. Helv.*, 83, 311–321, 1990.

881 Koutsodendris, A., Pross, J., Müller, U. C., Brauer, A., Fletcher, W. J., Kühl, N., Kirilova, E., Verhagen,  
882 F. T., Lücke, A., and Lotter, A. F.: A short-term climate oscillation during the Holsteinian  
883 interglacial (MIS 11c): An analogy to the 8.2ka climatic event?, *Global Planet. Chang.*, 92–93,  
884 224–235, <https://doi.org/10.1016/j.gloplacha.2012.05.011>, 2012.

885 Krohn, C. F., Larsen, N. K., Kronborg, C., Nielsen, O. B., and Knudsen, K.: L. Litho- and  
886 chronostratigraphy of the Late Weichselian in Vendyssel, northern Denmark, with special  
887 emphasis on tunnel-valley infill in relation to a receding ice margin. *Boreas*, 38, 811–833,  
888 <https://doi.org/10.1111/j.1502-3885.2009.00104.x>, 2009.

889 Kühni, A., and Pfiffner, O.A.: The relief of the Swiss Alps and adjacent areas and its relation to lithology  
890 and structure: topographic analysis from a 250-m DEM. *Geomorphology*, 41, 285–307,  
891 [https://doi.org/10.1016/S0169-555X\(01\)00060-5](https://doi.org/10.1016/S0169-555X(01)00060-5), 2001.

892 Liebl, M., Robl, J., Hergarten, S., Egholm, D.L., and Stüwe, K.: Modeling large-scale landform  
893 evolution with a stream power law for glacial erosion (OpenLEM v37): benchmarking  
894 experiments against a more process-based description of ice flow (iSOSIA v3.4.3). *Geosci.*  
895 *Model Dev.*, 16, 1315–1343, <https://doi.org/10.5194/gmd-16-1315-2023>, 2023.

896 Lloyd, C., Clark, C.D., and Swift, D.A.: The effect of valley confluence and bedrock geology upon the  
897 location and depth of glacial overdeepenings. *Geogr. Ann.: Series A, Phys. Geogr.*,  
898 <https://doi.org/10.1080/04353676.2023.2217047>, 2023.

899 Lohrberg, A., Schneider von Deimling, J., Grob, H., Lenz, K.-F., and Krastel, S.: Tunnel valleys in the  
900 southeastern North Sea: More data, more complexity. *E&G Quat. Sci. J.*, 71, 267–274,  
901 <https://doi.org/10.5194/egqsj-71-267-2022>, 2022.

902 Lüthy, H., Matter, A., and Nabholz, W.K.: Sedimentologische Untersuchungen eines temporären  
903 Quartäraufschlusses bei der Neubrügg nördlich Bern. *Eclogae Geol. Helv.*, 56, 119–145,  
904 <https://doi.org/10.5169/seals-163032>, 1963.

905 Magrani, F., Valla, P.G., Gribenski, N., and Serra, E.: Glacial overdeepening in the Swiss Alps and  
906 foreland: Spatial distribution and morphometrics. *Quat. Sci. Rev.*, 243, 106483,  
907 <https://doi.org/10.1016/j.quascirev.2020.106483>, 2020.

908 Magrani, F., Valla, P.G., and Egholm, D.: Modelling alpine glacier geometry and subglacial erosion  
909 patterns in response to contrasting climatic forcing. *Earth Surf. Process. Landf.*, 47, 1954–1072,  
910 <https://doi.org/10.1002/esp.5302>, 2022.

Formatted: English (UK)

Field Code Changed

Field Code Changed

Field Code Changed

Formatted: German (Switzerland)

Formatted: German (Switzerland)

Formatted: German (Switzerland)

Formatted: English (UK)

Formatted: English (UK)

Formatted: English (UK)

Formatted: English (UK)

911 Moreau, J., Huuse, M., Janszen, A., van der Vegt, P., Gibbard, P. L., and Moscriello, A.: The  
912 glaciogenic unconformity of the southern North Sea. *Geol. Soc. London Spec. Publ.*, 368, 99,  
913 <https://doi.org/10.1144/SP368.5>, 2012.

914 Montgomery, D. R., and Korup, O.: Preservation of inner gorges through repeated Alpine glaciations.  
915 *Nat. Geosci.*, 4, 62-67, <https://doi.org/10.1038/Ngeo1030>, 2011.

916 Nagy, D.: The gravitational attraction of a right rectangular prism. *Geophyscis*, 31, 362–271, 1996.

917 Nishiyama, R., Ariga, A., Ariga, T., Lechmann, A., Mair, D., Pistillo, C., Scampoli, P., Valla, P.G.,  
918 Vladymyrov, M., Ereditato, A., and Schlunegger, F.: Bedrock sculpting under an active alpine  
919 glacier revealed from cosmic-ray muon radiography. *Sci. Rep.*, 9, 6970,  
920 <https://doi.org/10.1038/s41598-019-43527-6>, 2019.

921 Olivier, R., Dumont, B., and Klingele, E.: Carte gravimétrique de la Suisse (Anomalies de Bouguer)  
922 1:500'000. Bundesamt für Landestopographie swisstopo,  
923 <https://opendata.swiss/fr/dataset/schwerekarte-der-schweiz-bouguer-anomalien-1-500000>,  
924 2008, 2011.

925 Ottesen, D., Stewart, M., Brønner, M., and Batchelor, C. L.: Tunnel valleys of the central and northern  
926 North Sea (56°N to 62°N): Distribution and characteristics. *Mar. Geol.*, 425, 106199,  
927 <https://doi.org/10.1016/j.margeo.2020.106199>, 2020.

928 Patton, H., Swift, D. A., Clark, C. D., Livingstone, S. J., and Cook, S. J.: Distribution and characteristics  
929 of overdeepenings beneath the Greenland and Antarctic ice sheets: Implications for  
930 overdeepening origin and evolution. *Quat. Sci. Rev.*, 148, 128–145,  
931 <https://doi.org/10.1016/j.quascirev.2016.07.012>, 2016.

932 Pedersen, V.K., and Egholm, D.L.: Glaciations in response to climate variations preconditioned by  
933 evolving topography. *Nature*, 493, 206-201, <https://doi.org/10.1038/nature11786>, 2013.

934 Perrouty, S., Moussirou, B., Martinod, J., Banvalot, S., Carretier, S., Gabalda, G., Monod, B., Hérail,  
935 G., Regard, V., and Remy, D.: Geometry of two glacial valleys in the northern Pyrenees  
936 estimated using gravity data, *Comptes Rendus Geosci.*, 347, 13–23,  
937 <https://doi.org/10.1016/j.crte.2015.01.002>, 2015.

938 Piotrowski, J.A.: Subglacial hydrology in north-western Germany during the last glaciation:  
939 Groundwater flow, tunnel valleys and hydrological cycles. *Quat. Sci. Rev.*, 16, 169-185,  
940 [https://doi.org/10.1016/S0277-3791\(96\)00046-7](https://doi.org/10.1016/S0277-3791(96)00046-7), 1997.

941 Platt, N., and Keller, B.: Distal alluvial deposits in a foreland basin setting – the Lower Freshwater  
942 Molasse (Lower Miocene), Switzerland: sedimentology, architecture and palaeosols.  
943 *Sedimentology*, 39, 545-565, <https://doi.org/10.1111/j.1365-3091.1992.tb02136.x>, 1992.

944 Preusser, F., and Schlüchter, C. Dates from an important early Late Pleistocene ice advance in the Aare  
945 valley, Switzerland. *Eclogae Geol. Helv.*, 97, 245–253, [https://doi.org/10.1007/s00015-004-](https://doi.org/10.1007/s00015-004-1119-4)  
946 1119-4, 2004.

Field Code Changed

Field Code Changed

Formatted: English (UK)

Field Code Changed

Formatted: English (UK)

Formatted: English (UK)

Field Code Changed

Field Code Changed

Field Code Changed

Field Code Changed

Field Code Changed



947 Preusser, F., Drescher-Schneider, R., Fiebig, M., and Schlüchter, C.: Re-interpretation of the Meikirch  
948 pollen record, Swiss Alpine Foreland, and implications for Middle Pleistocene  
949 chronostratigraphy. *J. Quat. Sci.*, 20., 607-620, <https://doi.org/10.1002/jqs.930>, 2005.

950 Preusser, F., Reitner, J. M., and Schlüchter, C.: Distribution, geometry, age and origin of overdeepened  
951 valleys and basins in the Alps and their foreland. *Swiss J. Geosci.*, 103, 407-426,  
952 <https://doi.org/10.1007/s00015-010-0044-y>, 2010.

953 Preusser, F., Graf, H. R., Keller, O., Krayss, E., and Schlüchter, C.: Quaternary glaciation history of  
954 Northern Switzerland. *E&G Quat. Sci. J.*, 60, 282-305, <https://doi.org/10.3285/eg.60.2-3.06>,  
955 2011.

956 Reber, R., and Schlunegger, F.: Unravelling the moisture sources of the Alpine glaciers using tunnel  
957 valleys as constraints. *Terra Nova*, 28, 202-211, <https://doi.org/10.1111/ter.12211>, 2016.

958 Reitner, J.M., Gruber, W., Römer, A., and Morawetz, R.: Alpine overdeepenings and paleo-ice flow  
959 changes: an integrated geophysical-sedimentological case study from Tyrol (Austria). *Swiss J.*  
960 *Geosci.*, 103, 385-405, <https://doi.org/10.1007/s00015-010-0046-9>, 2010.

961 Roger, S., Féraud, G., de Beaulieu, J.-L., Thouveny, N., Coulon, Ch., Choucem., J.J., Andrieu, V. and  
962 Williams, T.: 40Ar/39Ar dating on tephra of the Velay maars (France): implications for the  
963 Late Pleistocene proxy-climatic record. *Earth Planet Sci. Lett.*, 170: 287-299, 1999.

964 Ross, N., Siegert, M.J., Woodward, J., Smith, A.M., Corr, H.F.J., Bentley, M.J., Hindsmarsh, R.C.A.,  
965 King, E.C., and Rivera, A.: Holocene stability of the Amundsen-Weddell ice divide, West  
966 Antarctica. *Geology*, 39, 935-938, <https://doi.org/10.1130/G31920>, 2011.

967 Rosselli, A., and Raymond, O. : Modélisation gravimétrique 2.5D et cartes des isohypses au 1:100'000  
968 du substratum rocheux de la Vallée du Rhône entre Villeneuve et Brig (Suisse). *Eclogae Geol.*  
969 *Helv.*, 96, 399-423, 2003.

970 Schaller, S., Büchi, M.W., Schuster, B., and Anselmetti, F.: Drilling into a deep buried valley (ICDP  
971 DOVE): a 252 m long sediment succession from a glacial overdeepening in northwestern  
972 Switzerland. *Sci. Drill.*, 32, 27-42, <https://doi.org/10.5194/sd-32-27-2023>, 2023.

973 Schläfli, P., Gobet, E., van Leeuwen, J.F.N., Vescovi, E., Schwenk, M.A., Bandou, D., Douillet, G.A.,  
974 Schlunegger, F., and Tinner, W.: Palynological investigations reveal Eemian interglacial  
975 vegetation dynamics at Spiezberg, Bernese Alps, Switzerland. *Quat. Sci. Rev.*, 263, 106975,  
976 <https://doi.org/10.1016/j.quascirev.2021.106975>, 2021.

977 Schlüchter, C.: Thalgut: ein umfassendes eiszeitstratigraphisches Referenzprofil im nördlichen  
978 Alpenvorland. *Eclogae geol. Helv.*, 82, 277-284, 1989.

979 Schlüchter, C. The Swiss glacial record – a schematic summary. *Develop. Quat. Sci.*, 2, 413-418,  
980 [https://doi.org/10.1016/S1571-0866\(04\)80092-7](https://doi.org/10.1016/S1571-0866(04)80092-7), 2004.

981 Schlunegger, F., and Garefalakis, P.: Einführung in die Sedimentologie, Schweizerbart, Stuttgart,  
982 [www.schweizerbart.de/9783510655397](http://www.schweizerbart.de/9783510655397), 2023.

Field Code Changed

Field Code Changed

Field Code Changed

Field Code Changed

Field Code Changed

Formatted: English (UK)

Field Code Changed

Formatted: English (UK)

983 [Schuster, B., Gegg, L., Schaller, S., Buechi, M., Tanner, D.C., Wielandt-Schuster, U., Anselmetti, F.,](#)  
984 [and Preusser, F.: Shaped and filled by the Rhine Glacier: the overdeepened Tannwald Basin in](#)  
985 [southwestern Germany. Sci. Drill., 33, 191-206. <https://doi.org/10.5194/sd-33-191-2024>, 2024.](#)  
986 Schwenk, M., Schläfli, P., Bandou, D., Gribenski, N., Douillet, G., and Schlunegger, F.: From glacial  
987 erosion to basin overfill: A 240 m-thick overdeepening-fill sequence in Bern, Switzerland. Sci.  
988 Drill., 30, 17–42, <https://doi.org/10.5194/sd-30-17-2022>, 2022a.  
989 Schwenk, M. A., Stutenbecker, L., Schläfli, P., Bandou, D., and Schlunegger, F.: Two glaciers and one  
990 sedimentary sink: The competing role of the Aare and the Valais glaciers in filling an  
991 overdeepened trough inferred from provenance analysis. E&G Quat. Sci. J., 71, 163–190,  
992 <https://doi.org/10.5194/egqsj-71-163-2022>, 2022b.  
993 Stäger, D., Labhart, T., Della Valle, G., Tröhler, B., Schwarz, H., Gisler, C., Rathmayr, B. and  
994 Wiederkehr, M. Blatt 1210 Innertkirchen. Geol. Atlas Schweiz 1:25'000, Karte 167, Swisstopo,  
995 2020.  
996 Steinemann, O., Ivy-Ochs, S., Hippe, K., Christl, M., Naghipour, N., and Synal, H.-A.: Glacial erosion  
997 by the Trift glacier (Switzerland): Deciphering the development of riegels, rock basins and  
998 gorges. *Geomorphology*, 375, 107533, <https://doi.org/10.1016/j.geomorph.2020.107533>, 2021.  
999 Stewart, M.A., and Lonergan, L.: Seven glacial cycles in the middle-late Pleistocene of northwest  
1000 Europe: geomorphic evidence from buried tunnel valleys. *Geology* 39, 283-286,  
1001 <https://doi.org/10.1130/G31631.1>, 2011.  
1002 Stewart, M.A., Lonergan, L. and Hampson, G.: 3D seismic analysis of buried tunnel valleys in the  
1003 central North Sea: tunnel valley-fill sedimentary architecture, in: *Glaciogenic Reservoirs and*  
1004 *Hydrocarbon Systems*, edited by: Huuse, M., Redfern, J., Le Heron, D.P., Dixon, R.J., and  
1005 Moscardiello, A.. *Geol. Soc. London Spec. Publ.*, 368, 173-183,  
1006 <http://dx.doi.org/10.1144/SP368.9>, 2013.  
1007 Valla, P.G., van der Beek, P.A., and Carcaillet, J.: Dating bedrock gorge incision in the French Western  
1008 Alps (Ecrins-Pelvoux massif) using cosmogenic <sup>10</sup>Be. *Terra Nova*, 22, 18-25,  
1009 <https://doi.org/10.1111/j.1365-3121.2009.00911.x>, 2010.  
1010 Valla, P., Shuster, D.L., and van der Beek, P.A.: Significant increase in relief of the European Alps  
1011 during mid-Pleistocene glaciations. *Nat. Geosci.*, 4, 688-692,  
1012 <https://doi.org/10.1038/ngeo1242>, 2011.  
1013 Welten, M.: Pollenanalytische Untersuchungen im jüngeren Quartär des nördlichen Alpenvorlandes der  
1014 Schweiz. *Beitr. Geol. Karte Schweiz*, 156, 174 pp., 1982.  
1015 Welten, M.: Neue pollenanalytische Ergebnisse über das jüngere Quartär des nördlichen  
1016 Alpenvorlandes der Schweiz (Mittel-und Jungpleistozän). *Beitr. Geol. Karte Schweiz*, 162, 9-  
1017 40, 1988.

Field Code Changed

Formatted: English (UK)

Field Code Changed

Field Code Changed

Formatted: English (UK)

- 1018 Wright, H. E.: Tunnel valleys, glacial surges, and subglacial hydrology of the Superior Lobe, 340  
1019 Minnesota. Mem. Geol. Soc. Amer., 136, 251-276, <https://doi.org/10.1130/MEM136-p251>,  
1020 1973.
- 1021 Zwahlen, P., Tinner, W. and Vescovi, E.: Ein neues EEM-zeitliches Umweltarchiv am Spiezberg  
1022 (Schweizer Alpen) im Kontext der mittel- und spätpleistozänen Landschaftsentwicklung. Mitt.  
1023 Naturf. Ges. Bern 78, 92–121, 2021.

Formatted: English (UK)